Computational challenges in Astrochemistry

Malgorzata Biczysko,[1] Julien Bloino[2,3] and Cristina Puzzarini[4]*

Cosmic evolution is the tale of progressive transition from simplicity to complexity. The newborn universe starts with the simplest atoms formed after the Big Bang and proceeds toward 'astronomical complex organic molecules' (astroCOMs). Understanding the chemical evolution of the universe is one of the main aims of Astrochemistry, with the starting point being the knowledge whether a molecule is present in the astronomical environment under consideration and, if so, its abundance. However, the interpretation of astronomical detections and the identification of molecules are not all straightforward. In particular, molecular species characterized by large amplitude motions represent a major challenge for molecular spectroscopy and, in particular, for computational spectroscopy. More in general, for flexible systems, the conformational equilibrium needs to be taken into account and accurately investigated. It is shown that crucial challenges in the computational spectroscopy of astroCOMs can be successfully overcome by combining state-of-the-art quantum-mechanical approaches with *ad hoc* treatments of the nuclear motion, thus demonstrating that the rotational and vibrational features can be predicted with the proper accuracy. The second key step in Astrochemistry is understanding how astroCOMs are formed and how they chemically evolve toward more complex species. The challenges in the computational chemistry of astroCOMs are related to the derivation of feasible formation routes in the typically harsh conditions (extremely low temperature and density) of the interstellar medium, as well as the understanding of the chemical evolution of small species toward macromolecules. Within the transition state theory, for instance, it is possible to obtain new astrochemical information by identifying the intermediate species and transition states connecting them in a plausible formation route. Depending on the sophistication of the model, different quantities may be needed. Nevertheless, accuracy can be critical, thus requiring state-of-the-art computational approaches to derive geometries, energies, spectroscopic properties, and thermochemical data for each relevant structure along the reaction path. © 2017 Wiley Periodicals, Inc.

*Correspondence to: cristina.puzzarini@unibo.it

[1]International Center for Quantum and Molecular Structures, College of Sciences, Shanghai University, Shanghai, China

[2]Consiglio Nazionale delle Ricerche, Istituto di Chimica dei Composti OrganoMetallici, UOS di Pisa, Area della Ricerca CNR, Pisa, Italy

[3]Scuola Normale Superiore, Classe di Scienze, Pisa, Italy

[4]Department of Chemistry "Giacomo Ciamician", University of Bologna, Bologna, Italy

Conflict of interest: The authors have declared no conflicts of interest for this article.

INTRODUCTION: THE INTERSTELLAR MOLECULAR COMPLEXITY

For many years, the interstellar medium (ISM) was considered too hostile for organic species to be formed. However, roughly 40 years ago, the first molecules containing carbon chains and rings were discovered. With time, a rapidly increasing number of molecules of noteworthy complexity have been observed in space. Indeed, the detection of over 200 molecules, with almost all of them observed

unambiguously in the ISM or circumstellar shells and about 60 molecules detected in extragalactic sources (see, e.g., the Cologne Database for Molecular Spectroscopy, CDMS)[1,2] suggests that the ISM is characterized by a rich chemistry. Understanding the chemical evolution of the universe is one of the main aims of Astrochemistry,[3,4] with the starting point being the knowledge whether a molecule is present in the astronomical environment under consideration and, if so, its abundance. The second step is understanding how these molecular species are formed and how they evolve chemically toward more complex species. In this scenario, molecular spectroscopy and computational chemistry play a crucial role.[5–13] On one side, astronomical observations of spectroscopic signatures provide the unequivocal proof of the presence of chemical species; on the other side, quantum chemistry allows shedding light on their formation/transformation mechanisms, which are nowadays still object of debate and often not experimentally investigatable.

Similarly to astronomical observations that started with the detection of the smallest di-/triatomic molecules, the computational support in the field of Astrochemistry began with highly accurate theoretical predictions of rovibrational transitions of small (di- and triatomic) molecules, thus leading to extended line lists, which are important for the study of hot atmospheres, particularly those of exoplanets, brown dwarfs, and cool stars.[14,15] However, new challenges are posed by the large amount of data that nowadays need to be analyzed. In fact, the advent of large instantaneous bandwidth receivers characterized by high spectral resolution has opened up the possibility of large spectral surveys with a uniform sensitivity. If, on one hand, they are clearly the ideal mean to obtain a complete census of the species emitting in the recorded spectral survey, on the other hand, their identification is particularly challenging, thus requiring the increasing support from laboratory (both experimental and theoretical) studies. In fact, thanks to these new devices, it is now possible to explore extensively areas where reference experimental laboratory data are lacking.

Among others, the ultimate goal of the detection of prebiotic and biological molecules in astrochemical environments is one of the most appealing challenges of Astrochemistry.[16] In recent years, the Prebiotic Interstellar Molecular Survey (PRIMOS) project at the Green Bank Telescope (GBT)[17,18] contributed to the detection of over a dozen of new interstellar molecules (containing 6 to 11 atoms), including the first example of chiral molecule, methyloxirane.[19] In view of the opportunities opened by the Atacama Large Millimeter/submillimeter Array (ALMA) of radiotelescopes, working in the 31–950 GHz frequency range, and by the Mid-Infrared Instrument (MIRI), part of the James Webb Space Telescope (JWST, to be launched in 2018), it is necessary to extend reference data to reach higher frequencies to support astronomical observations. To give an idea, the rotational signatures of molecules showing a certain degree of complexity are often obtained from low-frequency laboratory measurements, well below 100 GHz. Moreover, even for small and widely investigated molecules, experimental studies have not yet completely and unequivocally determined the whole far-to-mid range infrared (IR) spectrum, with some bands (even including fundamental transitions) still missing or not measured with sufficient accuracy or in isolated, 'space-like' conditions.[20] Finally, emission spectra of relevance to astrochemical studies for samples composed of mixtures of unknown components are still quantitatively resolved only for a limited number of bands.

The focus of the present review is on the quantum-chemical support to the investigation of the so-called astronomical complex organic molecules, hereinafter referred to as astroCOMs, which are molecules containing at least six atoms, including carbon, hydrogen and, in most cases, at least another heavy element. Examples of astroCOMS, discussed in more details in the following, are gathered in Figure 1. Even if aminoacids and nucleobases have been found in meteorites (see Refs 27 and 28), they have not yet been unequivocally observed in the ISM, clearly showing the importance of improved reference spectroscopic data for their detection in different space environments. In this respect, it is encouraging that nowadays it is possible to evaluate structural, thermodynamic, and spectroscopic properties of medium-sized molecules with an accuracy that, until recently, could be reached only for very small rigid systems.[29–32] Highly accurate results can be nowadays obtained by means of composite and/or hybrid models (the reader is referred to their definition provided later in the manuscript), thus paving the route toward the complete spectroscopic characterization of astroCOMs to be then detected in the ISM through their rotational and vibrational features.[16,32] We will discuss the successful strategies that allow the determination of bond distances, rotational constants, conformational enthalpies, and vibrational wavenumbers with accuracies better than 0.001 Å, 20 MHz, 1 kJ mol^{-1} and 10 cm^{-1}, respectively. Particular emphasis will be put on the cases illustrating that theoretical data allow to reassess astronomical observations and providing new

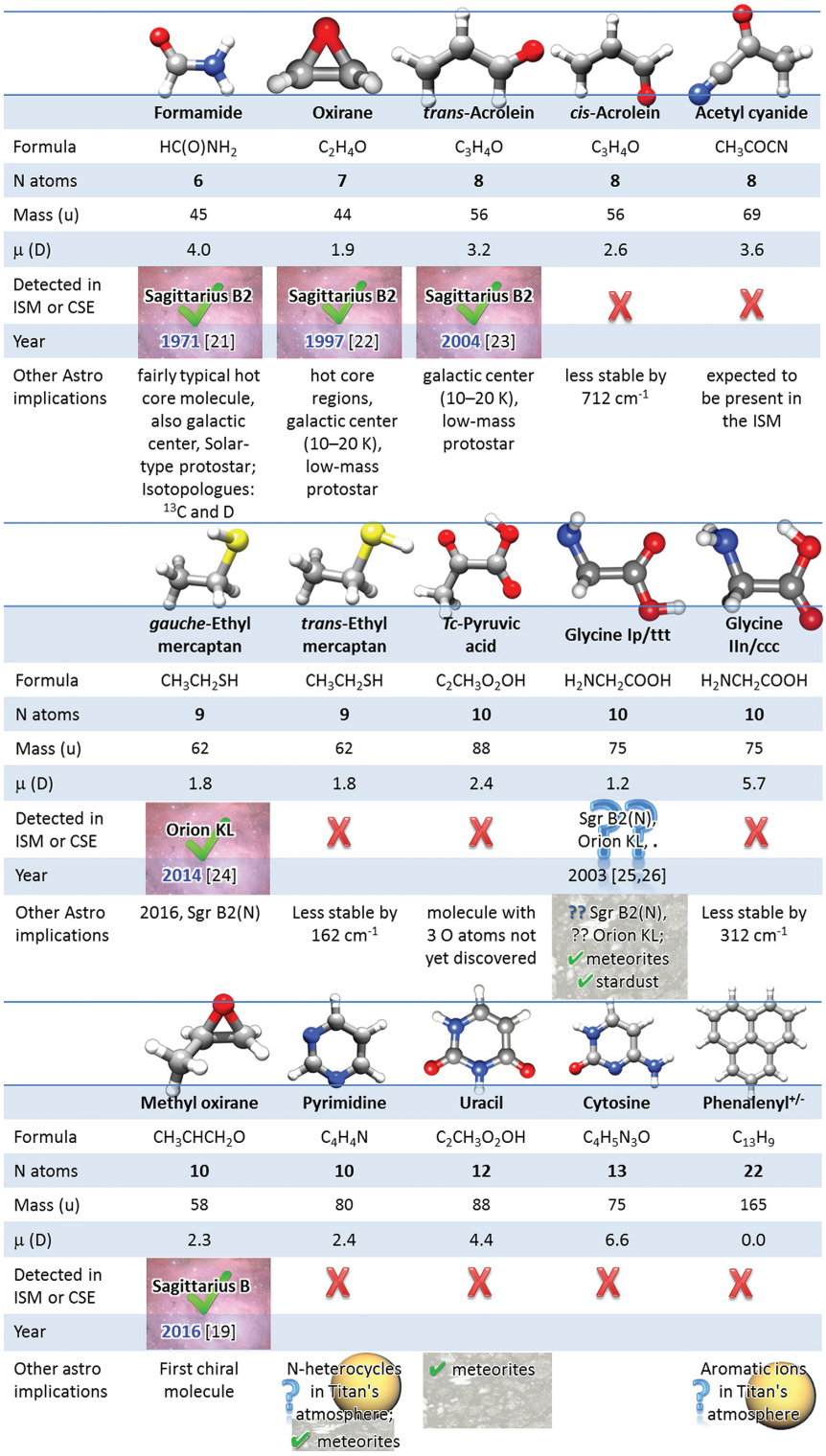

FIGURE 1 | The astroCOMs (or potential astroCOMs) addressed in this review: molecular formula and structure together with the relevant information.[1,2,19,21–26]

insights on possible discoveries of yet-undetected astroCOMs.[16,20] Possible pathways to overcome some of the remaining challenges related to the molecular complexity and flexibility, which are due to the conformational equilibria and large amplitude motions (LAMs), will be also discussed. The same

theoretical schemes can be also applied to the investigation of the chemical evolution,[33] thus allowing for reliable thermochemical and kinetic information on the formation processes of astroCOMs in various environments, including cold interstellar clouds.

COMPUTATIONAL SPECTROSCOPY OF ASTROCOMS

As already mentioned, more than 200 molecules have been detected in space.[1,2] Our knowledge on the universe chemical inventory has been obtained and continuously updated by means of astronomical observations, which have revealed a plethora of molecular species,[34] thus demonstrating the rich chemistry of the universe. Molecules can exist in a wide range of astrophysical environments, from the extremely cold regions between stars to the atmospheres of stars themselves. Focusing on their detection, the spectroscopic techniques of interest are rotational and IR spectroscopies. In fact, gas-phase species have been mostly discovered via their rotational signatures, with the corresponding frequencies going from the millimeter-wave region up to far infrared (FIR). However, spectroscopies in the IR domain play a crucial role, for example, in the investigation of planetary atmospheres.

As a preliminary remark, we should emphasize the fact that many different theoretical models have been proposed in the literature for the computation of spectroscopic properties, ranging from exact treatments of nuclear motions in conjunction with highly accurate potential energy surfaces (PESs)[15,35–39] to more practical methods.[40] Regarding the methodologies applicable to astroCOMs for their spectroscopic characterization, two popular approaches, either based on variational[41–44] or perturbative[45–66] schemes should be mentioned, with several programs offering the possibility of performing anharmonic rovibrational calculations, at different levels of sophistication.[37,41,54,67–75] The approach chosen in the present review is based on vibrational perturbation theory (VPT). To have a better understanding of the challenges to face in accurate calculations on molecular systems of interest in Astrochemistry, let us first recall some key aspects of the underlying theory, with special reference to spectroscopic parameters and nuclear motion effects.

Theory

First, we will assume that the Born–Oppenheimer approximation stands, so the electronic and nuclear degrees of freedom can be separated. For our purposes, the rovibrational Hamiltonian, $\mathcal{H}_{\text{rovib}}$, will be defined as follows[76]:

$$\mathcal{H}_{\text{rovib}} = \frac{\hbar^2}{2hc}\sum_{\tau,\eta}\mu_{\tau\eta}(J_\tau - \pi_\tau)(J_\eta - \pi_\eta) + \frac{1}{2}\sum_{i=1}^{N}\omega_i {p_i}^2 + V + U \tag{1}$$

where τ and η are Cartesian axes of the molecule-fixed frame, $\boldsymbol{\mu}$ is the effective inverse molecular inertia tensor, and $\boldsymbol{J}$ and $\boldsymbol{\pi}$ are, respectively, the rotational and vibrational angular momentum operators. V is the potential energy operator and U is a mass-dependent contribution

$$U = -\frac{\hbar^2}{8hc}\sum_{\tau}\mu_{\tau\tau} \tag{2}$$

which vanishes for linear systems. The form of the vibrational angular momentum operator $\boldsymbol{\pi}$ is

$$\pi = \sum_{i,j=1}^{N}\zeta_{ij}\sqrt{\frac{\omega_i}{\omega_j}}q_i p_j \tag{3}$$

In the equations above, $\boldsymbol{q}$ and $\boldsymbol{p}$ refer to the vectors of the dimensionless normal coordinates and their conjugate momenta, respectively. N is the number of vibrational normal modes ($N = 3N_a - 5$ for linear systems, $N = 3N_a - 6$ otherwise, with N_a the number of atoms). Finally, $\boldsymbol{\zeta}$ is the matrix of Coriolis couplings.

Both $\boldsymbol{\mu}$ and V can be expanded as Taylor series of the normal coordinates $\boldsymbol{q}$ about the equilibrium geometry[77]:

$$\begin{aligned}\mu_{\tau\eta} = {} & \mu_{\tau\eta}^{\text{eq}} - \sum_{i=1}^{N}\mu_{\tau\tau}^{\text{eq}}\mathrm{a}_{i,\tau\eta}\mu_{\eta\eta}^{\text{eq}}q_i \\ & + \frac{3}{4}\sum_{\varsigma}\sum_{i,j=1}^{N}\mu_{\tau\tau}^{\text{eq}}\mathrm{a}_{i,\tau\varsigma}\mu_{\varsigma\varsigma}^{\text{eq}}\mathrm{a}_{j,\varsigma\eta}\mu_{\eta\eta}^{\text{eq}}q_i q_j \\ & + \cdots\end{aligned} \tag{4}$$

$$\begin{aligned}V = {} & \frac{1}{2}\sum_{i=1}^{N}\omega_i {q_i}^2 + \frac{1}{6}\sum_{i,j,k=1}^{N}\mathrm{k}_{ijk}q_i q_j q_k \\ & + \frac{1}{24}\sum_{i,j,k,l=1}^{N}\mathrm{k}_{ijkl}q_i q_j q_k q_l + \cdots\end{aligned} \tag{5}$$

with

$$\mathrm{a}_{i,\tau\eta} = \frac{\partial \mathrm{I}_{\tau\eta}^{\text{eq}}}{\partial q_i}$$

$$\mathrm{k}_{ijk} = \frac{\partial^3 V}{\partial q_i \partial q_j \partial q_k}$$

$$\mathrm{k}_{ijkl} = \frac{\partial^4 V}{\partial q_i \partial q_j \partial q_k \partial q_l}$$

k_{ijk} and k_{ijkl} are commonly referred to as the cubic and quartic force constants, respectively, $\boldsymbol{I}^{\mathrm{eq}}$ is the equilibrium molecular inertia tensor, and ω_i is the harmonic wavenumber of mode *i*.

Once $\boldsymbol{\mu}$ and V in Eq. (1) are replaced by their Taylor expansions, it is possible to recast the rovibrational Hamiltonian as a series of terms $\mathcal{H}_{fg}$ based on the powers f of the vibrational operators ($\boldsymbol{q}$ and $\boldsymbol{p}$) and g of the rotational operators ($\boldsymbol{J}$):

$$\begin{aligned}\mathcal{H}_{\mathrm{rovib}} = {} & \mathcal{H}_{20} + \mathcal{H}_{30} + \mathcal{H}_{40} + \ldots \\ & + \mathcal{H}_{21} + \mathcal{H}_{31} + \mathcal{H}_{41} + \ldots \\ & + \mathcal{H}_{02} + \mathcal{H}_{12} + \mathcal{H}_{22} + \ldots\end{aligned} \tag{6}$$

For the sake of clarity, the subscript "rovib" has been dropped in the right-hand side of this definition. In the following, we will also assume that the molecule is oriented in such a way that its principal moments of inertia are collinear with the Cartesian axes of the reference frame, the so-called Eckart orientation,[78] in order to minimize the vibrational-rotational couplings. Under this condition, the equilibrium effective inverse molecular inertia tensor $\boldsymbol{\mu}^{\mathrm{eq}}$ can be replaced by the equilibrium molecular rotational constants vector $\boldsymbol{B}^{\mathrm{eq}}$ defined as

$$B_\tau^{\mathrm{eq}} = \frac{\hbar^2}{2hc\mathrm{I}_{\tau\tau}^{\mathrm{eq}}} \tag{7}$$

In order to derive analytic formulas for the simulation of rotational and vibrational spectra, two major formalisms can be followed, namely the Rayleigh-Schrödinger perturbation theory and the van Vleck contact transformation (CT).[49,79] The latter is based on the transformation of the Schrödinger equation, with the Hamiltonian redefined as:

$$\widetilde{\mathcal{H}} = e^{iS}\mathcal{H}e^{-iS} \tag{8}$$

where S is a Hermitian operator so that e^{iS} is unitary.

$\widetilde{\mathcal{H}}$ is diagonal in a given basis ϕ, with the diagonal elements E being the eigenvalues of $\mathcal{H}$. What is of interest in this context is that the CT method gives a separation of the vibration-rotation Hamiltonian, which makes it possible to discuss the effective rotational Hamiltonian for an individual vibrational level, or a block of near-degenerate vibrational levels.

Rotational Hamiltonian

The terms $\widetilde{\mathcal{H}}_{0g}$, with g = 2, 4, 6…, in the effective Hamiltonian are the pure rotational and centrifugal-distortion contributions, which describe the rotational energy levels for the vibrational ground state. The complete treatment can be found in the literature[49]; here, we recall only the key aspects of interest.

As stated above, the vibrational CT leads to the rotational Hamiltonian

$$\widetilde{\mathcal{H}}_{rot} = \mathcal{H}_{02} + \widetilde{\mathcal{H}}_{04} + \widetilde{\mathcal{H}}_{06} \tag{9}$$

where $\widetilde{\mathcal{H}}_{04}$ and $\widetilde{\mathcal{H}}_{06}$ are the quartic and sextic centrifugal terms. $\mathcal{H}_{02} = \widetilde{\mathcal{H}}_{02}$ is the rigid-rotor Hamiltonian:

$$\mathcal{H}_{02} = \sum_\tau B_\tau^{\mathrm{eq}} J_\tau^2 \tag{10}$$

where B_τ^{eq} has been defined in Eq. (7). From a computational point of view, this is straightforwardly obtained from the geometry optimization. The quartic centrifugal-distortion Hamiltonian is defined as

$$\widetilde{\mathcal{H}}_{04} = \frac{1}{4}\sum_{\tau,\eta,\varsigma,\varrho} \tau_{\tau\eta\varsigma\varrho} J_\tau J_\eta J_\varsigma J_\varrho \tag{11}$$

where the tensor $\tau_{\tau\eta\varsigma\varrho}$ depends only on the harmonic part of the PES. To obtain the quartic centrifugal distortion parameters actually employed, further CTs with purely rotational operators (thus diagonal in the vibrational quantum numbers) are then required. The sextic centrifugal distortion constants are derived from the term $\widetilde{\mathcal{H}}_{06}$, which involves harmonic, anharmonic, and Coriolis perturbation terms for its calculation. Therefore, from a computational point of view, anharmonic force field computations are needed for their determination. To relate the experimental parameters to combinations of $\tau_{\tau\eta\varsigma\varrho}$ ($\tau_{\tau\eta\varsigma\varrho\epsilon\iota}$ in the case of sextics), it is necessary to further, completely reduce the Hamiltonian. Different results are then obtained depending on the reduction chosen.[49,80,81] To give an example, the rotational Hamiltonian up to the sextics for a rigid asymmetric-top molecule in the Watson A-reduction form[80,81] is:

$$\begin{aligned}\widetilde{\mathcal{H}}_{rot}^{(A)} = {} & \sum_\tau B_\tau^{(A)} J_\tau^2 - \Delta_J \left(J^2\right)^2 - \Delta_{JK} J^2 J_z^2 - \Delta_K J_z^4 \\ & - \frac{1}{2}\left[\left(\delta_J J^2 + \delta_K J_z^2\right), \left(J_+^2 + J_-^2\right)\right]_+ + \Phi_J \left(J^2\right)^3 \\ & + \Phi_{JK}\left(J^2\right)^2 J_z^2 + \Phi_{KJ} J^2 J_z^4 + \Phi_K J_z^6 \\ & + \frac{1}{2}\left[\left(\Phi_J \left(J^2\right)^2 + \Phi_{JK} J^2 J_z^2 + \Phi_K J_z^4\right), \left(J_+^2 + J_-^2\right)\right]\end{aligned} \tag{12}$$

where J^2 and $J_\pm$ are the total angular momentum and the ladder operators, respectively, with $[X, Y]_+$ representing the anticommutator. The Δ's and δ's are the quartic centrifugal distortion constants, while the Φ's and ϕ's are the sextic ones.[81]

The Hamiltonian given for example in Eq. (12) applies to the rigid-rotor approximation case. However, another important issue is the effect of molecular vibrations. The operators $\widetilde{\mathcal{H}}_{22}$, $\widetilde{\mathcal{H}}_{42}$, $\widetilde{\mathcal{H}}_{24}$, in Eq. (6) contain the terms describing the dependence of the rotational and centrifugal constants on the vibrational quantum numbers. The quantities multiplying J_τ^2 in Eq. (12) are actually the effective rotational constants and contain the contributions beyond the rigid-rotor harmonic-oscillator (RRHO) approximation. Their effects on rotational motion can be conveniently described by means of VPT, and we refer the reader to, for example, Refs 49 and 80 for a detailed treatment. While there are no corrections at the first order in VPT, at the second order (VPT2), three contributions appear that, expressed by means of the usual contact-transformation method,[49] give[47]:

$$B_\tau^v = B_\tau^{\mathrm{eq}} - \sum_{i=1}^{N} \alpha_{i,\tau}\left(v_i + \frac{d_i}{2}\right) \tag{13}$$

where the superscript v denotes a specific vibrational state and the sum is taken over all fundamental vibrational modes i, with v_i its quantum number and d_i its degeneracy order. The $\alpha_{i,\tau}$'s are the so-called vibration-rotation interaction constants and contain three contributions: the first one is a corrective term related to the moment of inertia, the second one is due to the Coriolis interactions, and the last is an anharmonic correction. Therefore, from a computational point of view, anharmonic force field calculations are required to correct the equilibrium rotational constants for vibrational effects.

Vibrational Hamiltonian

For the simulation of vibrational spectra, a purely vibrational Hamiltonian ($\mathcal{H}_{f0}$) is commonly used, which also includes the zeroth-order contribution from the effective inverse molecular inertia tensor:

$$\frac{\hbar^2}{2hc}\sum_{\tau,\eta}\mu_{\tau\eta}^{\mathrm{eq}}\pi_\tau\pi_\eta = \sum_\tau B_\tau^{\mathrm{eq}} \sum_{i,j,k,l=1}^{N} \zeta_{ij,\tau}\zeta_{kl,\tau}\sqrt{\frac{\omega_i\omega_k}{\omega_j\omega_l}}q_i p_j q_k p_l \tag{14}$$

As the name implies, the second-order VPT is based on Taylor expansions of the harmonic potential (V) and vibrational (ε) energies, as well as the vibrational wavefunction, up to the second order.[45] Considering the terms that are only functions of the normal coordinates or their conjugate momenta in Eq. (6), the vibrational Hamiltonian up to the fourth power of the operators of $\boldsymbol{q}$, $\boldsymbol{p}$ is then defined as

$$\mathcal{H}_{\mathrm{vib}} = \mathcal{H}_{20} + \mathcal{H}_{30} + \mathcal{H}_{40} \tag{15}$$

$$\begin{aligned}\mathcal{H}_{\mathrm{vib}} = {} & \frac{1}{2}\sum_{i=1}^{N}\omega_i\left(p_i^2 + q_i^2\right) + \frac{1}{6}\sum_{i,j,k=1}^{N}\mathrm{k}_{ijk}q_iq_jq_k \\ & + \frac{1}{24}\sum_{i,j,k,l=1}^{N}\mathrm{k}_{ijkl}q_iq_jq_kq_l \\ & + \sum_\tau B_\tau^{\mathrm{eq}}\sum_{i,j,k,l=1}^{N}\zeta_{ij,\tau}\zeta_{kl,\tau}\sqrt{\frac{\omega_i\omega_k}{\omega_j\omega_l}}q_ip_jq_kp_l + U\end{aligned} \tag{16}$$

Proper support of the normal modes degeneracy in VPT2 requires some specific treatments, thus leading to more complex formulas than for nondegenerate modes (see Ref 63 for a recent overview on the extension to symmetric and linear tops). For this reason, and to simplify the discussions, the normal mode degeneracy will be ignored in the following.

At the VPT2 level, a single formula is needed to compute the energy (ε_m, in cm^{-1}) of any vibrational state $|\, m \,\rangle$,

$$\varepsilon_m = \varepsilon_0 + \sum_{i=1}^{N} v_i^m\omega_i + \sum_{i,j=1}^{N}\chi_{ij}\left[v_i^m v_j^m + \frac{1}{2}\left(v_i^m + v_j^m\right)\right] \tag{17}$$

where v_i^m is the number of quanta associated to mode i in state $|\, m \,\rangle$ and ω_i its harmonic wavenumber. ε_0 is the zero-point vibrational energy (ZPVE), defined as

$$\begin{aligned}\varepsilon_0 = {} & \sum_{i=1}^{N}\frac{\omega_i}{2} + \sum_{i,j=1}^{N}\frac{\mathrm{k}_{iijj}}{32} - \sum_{i,j,k=1}^{N}\left[\frac{\mathrm{k}_{iik}\mathrm{k}_{jjk}}{32\omega_k} + \frac{\mathrm{k}_{ijk}{}^2}{48\left(\omega_i+\omega_j+\omega_k\right)}\right] \\ & - \sum_\tau\frac{B_\tau^{\mathrm{eq}}}{4}\left[1 - \sum_{i=1}^{N-1}\sum_{j=i+1}^{N}\left\{\zeta_{ij,\tau}\right\}^2\frac{\left(\omega_i-\omega_j\right)^2}{\omega_i\omega_j}\right]\end{aligned} \tag{18}$$

and $\boldsymbol{\chi}$ is the matrix containing the anharmonic contributions, with elements given by

$$16\chi_{ii} = \mathrm{k}_{iiii} - \frac{5\mathrm{k}_{iii}{}^2}{3\omega_i} - \sum_{\substack{j=1\\ j\neq i}}^{N}\frac{\left(8\omega_i{}^2 - 3\omega_j{}^2\right)\mathrm{k}_{iij}{}^2}{\omega_j\left(4\omega_i{}^2 - \omega_j{}^2\right)} \tag{19}$$

$$\begin{aligned}4\chi_{ij} = {} & \mathrm{k}_{iijj} - \frac{2\omega_i\mathrm{k}_{iij}{}^2}{\left(4\omega_i{}^2 - \omega_j{}^2\right)} - \frac{2\omega_j\mathrm{k}_{ijj}{}^2}{\left(4\omega_j{}^2 - \omega_i{}^2\right)} - \frac{\mathrm{k}_{iii}\mathrm{k}_{ijj}}{\omega_i} \\ & - \frac{\mathrm{k}_{jjj}\mathrm{k}_{iij}}{\omega_j} + \sum_{\substack{k=1\\ k\neq i,j}}^{N}\left[\frac{2\omega_k\left(\omega_i{}^2 + \omega_j{}^2 - \omega_k{}^2\right)\mathrm{k}_{ijk}{}^2}{\Delta_{ijk}}\right.\end{aligned}$$

$$-\frac{k_{iik}k_{jjk}}{\omega_k}\Bigg] + \frac{4\left(\omega_i^2+\omega_j^2\right)}{\omega_i\omega_j}\sum_\tau B_\tau^{eq}\left\{\zeta_{ij,\tau}\right\}^2 \qquad (20)$$

with

$$\Delta_{ijk} = \omega_i^4 + \omega_j^4 + \omega_k^4 - 2\left(\omega_i^2\omega_j^2 + \omega_i^2\omega_k^2 + \omega_j^2\omega_k^2\right)$$

Transition energies from the ground state are straightforwardly obtained from Eq. (17) as '$\nu_m = \varepsilon_m - \varepsilon_0$.'

Conversely, defining the anharmonic transition moments for the properties of interest (here the electric dipole) is more cumbersome for two major reasons. First, the property must also be expanded as a Taylor series, beyond the first-order derivative. This is referred to as the electrical anharmonicity, by contrast with the mechanical anharmonicity from the definition of the wavefunction. Next, at variance with the energy, it is not possible to derive a single, compact analytic formula, like Eq. (17), applicable to any transition. Multiple formulas are needed, depending on the number of quanta and excited modes separating the initial (generally the ground state) and final states (fundamental, first overtones, two-quanta combinations, and so on). Explicit equations for the transitions, including the properties function of the momenta conjugate of the normal coordinates, can be found in Refs 52,55,61,64,82. Instead of building compact formulas, an alternative, more general strategy is to build the integrals at runtime, during the calculations themselves, using either Rayleigh-Schrödinger[83] or van Vleck[57] formalisms. However, the computational cost and memory requirements to store the data necessary for the integrals are significantly higher than those required by the analytic forms. A presentation of their characteristic features is beyond the scope of the present contribution and will not be done here.

A quick inspection of Eqs. (19) and (20) is sufficient to identify simple conditions for which the VPT2 energies will be excessively high or even infinite, that is, when a denominator becomes very small. Those are known as Fermi resonances (FRs), divided in type I ($\omega_i \approx 2\omega_j$) and type II ($\omega_i \approx \omega_j + \omega_k$). Besides the limit case of an actual equality, which means that at least one element of the matrix $\boldsymbol{\chi}$ is infinite, a near resonance can be sufficient to obtain unphysical results due to an excessive contribution from anharmonicity. This is a well-known issue of VPT2, which has been extensively studied in the literature[49,53,56,60,84–94] and needs to be correctly addressed for a successful application of this method, *a fortiori* in the study of astroCOMs. A major difficulty lies in the definition of the resonance conditions. A very simple strategy to adopt is to define manually the resonances, based on the final vibrational energies. However, it does not scale well with the system size and is not sufficiently robust for a systematic use. A more efficient way is to automatize the identification process, which requires formalizing the concept of FRs. This can be achieved through different schemes.[53,56,60,63,85,87,92–94] A preliminary remark, which is also a reason for the variety of approaches proposed in the literature, is that most of them depend ultimately on thresholds defined empirically, thus introducing a degree of arbitrariness. However, this can be balanced to some extent by combining multiple criteria. A simple definition, and the starting point of many selection schemes, is the magnitude of the energy difference between the states (fundamental and two-quanta overtones or combinations) in the denominator. Such a basic test, however, neglects the magnitude of the overall term, which also depends on the cubic force field in the numerator. As a result, determining a single threshold applicable to every case is unpractical. A more robust solution is to complement this initial evaluation with a control of the magnitude of the potentially resonant term and its contribution to the anharmonic correction. We will mention here only the test proposed by Martin and coworkers, which is based on the deviation of this term from the energy of a model variational treatment of a system including only the two states involved in the resonance (for instance the states with harmonic energies 'ω_i' and '$\omega_j + \omega_k$' for a type II resonance).[85] More details can be found in the original paper. Terms identified as resonant are removed from the perturbative treatment for the calculation of the energy. This approach is named deperturbed VPT2 (DVPT2). However, this also means that the VPT2 treatment is truncated since terms are missing. This can be corrected through an *ad hoc* variational step, which reintroduces the previously discarded terms, using the DVPT2 vibrational energies as references. Different acronyms have been used to designate the overall procedure. Here, it is referred to as the generalized VPT2 (GVPT2). While GVPT2 is able to provide accurate results, it still relies directly on one or more empirical criteria for the identification of FRs. To reduce their impact, a two-step procedure is introduced here to select the resonances, the absolute frequency difference must be lower than a threshold Δ_ω^{1-2} and the deviation from the variational model must be higher than a chosen value K^{1-2}. In some cases, small variations in the

force constants (harmonic and anharmonic), like when employing different electronic structure calculation methods or by extracting a series of geometries along a reaction path, can be sufficient to modify the set of resonances, with a potentially notable impact on the final vibrational energies. An alternative way, proposed by Kuhler, Truhlar and Isaacson, is to replace every potentially resonant term with a nonresonant form derived from a model system comprising only the two states involved in each case.[86] A strong advantage of this method, denoted degeneracy-corrected PT2 (DCPT2), is that it does not use any threshold. However, the transformation is based on a number of approximations that lead to some inaccuracy for each replaced terms, which can be a problem far from resonance, where VPT2 behaves correctly. This shortcoming can be partially corrected by introducing a transition function which will mix the DCPT2 and VPT2 results for each potentially resonant terms, thus favoring VPT2 far from resonance. More details on this approach, called hybrid DCPT2-VPT2 (HDCPT2), can be found in Ref 60.

Finally, we should mention another type of resonances, collectively called Darling–Dennison resonances (DDRs).[53,57,58,63,87,89,94–97] This term describes couplings of states through the second-order vibrational Hamiltonian, not properly accounted for in the standard VPT2 theory. They originally refer to interactions between overtones, in particular for the CH and OH stretching modes, following the original study of Darling and Dennison on the water molecule.[95] The term has now a broader meaning and is also used to designate the so-called second-order interactions between fundamentals ('1–1'), two-quanta states ('2–2,' '2–11,' '11–11,' where '2' represents an overtone and '11' a combination), and fundamentals with three-quanta states ('1–3,' '1–21,' '1–111'), the last case being needed if three-quanta transitions are also included in the anharmonic calculations.[58,87] These resonances are commonly treated through a variational procedure, analogous to that used for FRs. In order to limit this step to relevant couplings, a two-step analysis similar to that introduced for FRs can be used, based on the absolute energy difference between the states (below a given threshold $\Delta_{\omega}^{\text{A-B}}$) and the magnitude of the off-diagonal term to be used in the variational step (higher than a chosen parameter, $K^{\text{A-B}}$). An hurdle specific to DDRs is the potential presence of FRs in the variational terms themselves. Depending on the method used for the identification of FRs in energy calculations, it may be possible or impractical to extend it straightforwardly to the case of DDRs. Further discussions on this problem can be found in Refs 87,94,98. In the following, GVPT2 will refer to the full variational treatment, including corrections to Fermi and Darling–Dennison resonances.

At variance, the problem of resonances in intensity calculations has been more scarcely addressed in the literature, to some extent due to the limited number of programs supporting them.[57,65,82,84,94] Since they are related to the mechanical anharmonicity (wavefunction), it is possible to use the analysis made for the energy on the transition moments as well. An important difference, however, is the impact of DDRs, which can lead to incorrect intensities if not accounted for properly, because the corresponding energy difference can directly appear at the denominator, in a way similar to FRs in energy calculations. This is especially important for modes or states (for three-quanta transitions) with near-equal harmonic energies, like for instance, the CH symmetric and antisymmetric stretching modes of a methyl group. Depending on the protocol followed for the definition of DDRs, it may be necessary to complement it with an *ad hoc* test targeted to handle the most critical cases (for instance of near-equal energies).[65,98] States coupled through a Darling–Dennison interaction need to be removed from the VPT2 formulas of the transition moments, thus resulting in fully deperturbed results where both FRs and DDRs are removed. These states are then projected on the GVPT2 states using the eigenvectors obtained from the energy calculation.[82]

From a computational perspective, for most of the examples chosen in this review, the suites of quantum chemical programs CFOUR[67] (high-level electronic structure methods, rotational spectroscopy) and GAUSSIAN[71] (density functional theory (DFT) computations, vibrational spectroscopy, thermodynamics, anharmonic contributions) have been used. Regarding VPT2 methods, vibrational energies and IR intensities have been calculated with GVPT2 and the thermodynamic properties with HDCPT2. Since simulations of fully anharmonic vibrational spectra have required the preceding computation of a semidiagonal quartic PES and a semidiagonal cubic property surface (PS), numerical differentiations along the normal coordinates of analytic harmonic force constants (for the PES) and first derivatives of the properties (for the PS) were carried out. Alternatively, methods to derive analytically all necessary derivatives have been proposed in the literature.[59,99–102] For the sake of completeness, it should be noted that both approaches mentioned here require a minimum order of derivation available analitically. This may not be the case depending on the electronic structure

calculation methods used or their actual implementation. A more general approach would be to carry out a multimode expansion, which can be tailored to the available quantities (see Refs 43,66,77 for details). Regarding the property of interest here, in the context of astroCOMs and the simulation of IR spectra, is the electric dipole moment.

Computational Methodology

The basic requirements for the theoretical support in the field of Astrochemistry are highly accurate predictions of the equilibrium molecular structures of astroCOMs, their rotational and vibrational spectroscopic parameters, and the abundance of different possible isomers or conformers for specific space-like conditions. To reach the target accuracy, the best possible quantum-mechanical (QM) methodologies must be employed in the description of the electronic structure, and then combined with solutions of the nuclear motion problem beyond the RRHO approximation. If, on one hand, electronic structure calculations should be pushed to the limit in order to determine very accurate equilibrium structures, on the other hand, it is also true that the harmonic part of the PES around the equilibrium needs to be described at the highest possible level. For a proper inclusion of the anharmonic effects in spectroscopic and thermodynamic properties, the force constants of Eq. (5) up to the fourth order need to be included as well, but a lower level of theory is sufficient for a high relative accuracy.[31,103,104]

The key point to obtain accurate results for the prediction of molecular structures and harmonic force fields is to reduce as much as possible the errors due to the truncation of both basis set and wavefunction, the so-called one- and N-electron errors, respectively. For this purpose, composite schemes that evaluate the contributions important to reach high accuracy at the best possible level and combine them through the additivity approximation have been set up.[105–110]

The so-called 'gradient' scheme,[108,109] implemented in the quantum-chemical program package CFOUR,[67] mainly involves calculations at the coupled cluster (CC) singles and doubles with perturbative triples corrections, CCSD(T), level.[111] However, the full CC singles, doubles, and triples (CCSDT)[112–114] and the CC singles, doubles, triples, quadruples (CCSDTQ)[115] models can also be employed. The correlation-consistent polarized cc-p(C)V*n*Z basis sets[116–119] are usually used in conjunction with this scheme. Within the 'gradient' scheme, the energy gradient to be minimized in the geometry optimization procedure is set up according to the specific needs, the target accuracy, and the dimension of the system under consideration. To recover the error due to the basis-set truncation, an extrapolation to the complete basis set (CBS) limit can be performed. Since extrapolation to the CBS limit is carried out within the frozen-core approximation, core-valence correlation (CV) effects are accounted for by adding the energy gradient corresponding to the difference of all-electron and frozen-core CCSD(T) calculations in the same basis set. In a similar manner, corrections from a full treatment of triples (fTs) and quadruples (fQs) can be included using small basis sets for their evaluation (usually of double-, triple-ζ quality). The overall energy gradient is given by the following expression:

$$\frac{dE_{\mathrm{CBS+core+fT+fQ}}}{dx} = \frac{dE^{\infty}(\mathrm{HF\text{-}SCF})}{dx} + \frac{d\Delta E^{\infty}(\mathrm{CCSD(T)})}{dx} + \frac{d\Delta E(CV)}{dx} + \frac{d\Delta E(\mathrm{full\text{-}T})}{dx} + \frac{d\Delta E(\mathrm{full\text{-}Q})}{dx} \tag{21}$$

From literature studies based on comparisons with experiment (see Refs 30,31,108,109,120–122 and references therein), the accuracy obtainable with the scheme presented above in terms of structural parameters is better than 0.001 Å for bonds and 0.1° for angles. It is particularly noteworthy that the loss of accuracy when the contributions from the fT and fQ excitations in the cluster expansion are ignored is very limited. The importance of this observation lies in the fact that, while the CCSD(T)/CBS + CV + fT + fQ level is computationally very expensive, the CCSD(T)/CBS + CV one is affordable also for medium-sized molecules, like glycine[29] and pyruvic acid.[30] In terms of geometrical parameters, the latter is well recognized to perform within 0.001–0.002 Å for distances and 0.05–0.1° for angles (see Refs 29,30,108,109,123). In Ref 110, the 'gradient' scheme was tested in terms of the accuracy reachable in predicting rotational constants, with the relevant results being summarized in Table 1. The overall conclusion is that the so-called CCSD(T)/CBS + CV level of theory leads to equilibrium rotational constants that agree well within 0.1% with experiment. However, Table 1 also points out that, for keeping the same accuracy when the comparison is performed with the experimental ground state rotational constants ($\boldsymbol{B}^0$), it is mandatory to include the vibrational corrections (see Eq. (13)).

To extend the applicability of composite approaches to larger molecules, an effective solution is provided by the so-called 'geometry' scheme, which is based on the assumption that the additivity

approximation can be directly applied to geometrical parameters and that they show the same behavior as the energy (see Refs 124–127). Analogously to the 'gradient' scheme, the various contributions are evaluated separately at the highest possible level and then combined in order to obtain best theoretical estimates. Unlike the 'gradient' scheme, which requires some specific software implementations to be used, the 'geometry' scheme is directly applicable and is definitely less computationally expensive. To further extend the size of systems amenable to accurate structural determinations, it is necessary to further reduce the computational cost. In recent years, a very effective approach, which mainly involves geometry optimizations using Møller–Plesset second-order theory (MP2)[128] and basis sets of triple- and quadruple-ζ quality, has been set up.[29,32,127,129] The starting point is the geometry optimization at the CCSD(T)/cc-pVTZ level within the frozen-core approximation, while all contributions required to improve its accuracy are computed at the MP2 level. As discussed in Refs 126 to take into account basis-set truncation effects, the CBS limit is evaluated by making use of the consolidated n^{-3} extrapolation form[130] applied to MP2/cc-pVTZ and MP2/cc-pVQZ optimized geometries. The effect due to core-valence electron correlation is included by means of the corresponding correction, Δr(CV), derived as the difference between the geometrical parameters optimized at the MP2/cc-pCVTZ level correlating all and only valence electrons. On the whole, within the 'geometry' scheme, the best-estimated (simply 'best' in the formula) equilibrium structure is determined as:

$$r(\text{best}) = r(\text{CCSD(T)/VTZ}) + \Delta r(\text{CBS}) + \Delta r(\text{CV}) + \Delta r(\text{aug}) \qquad (22)$$

This approach is denoted 'cheap' geometry scheme [31] to stress its reduced computational cost. While there is no theoretical justification for the inclusion of diffuse function effects (Δr(aug)) once the extrapolation to the CBS limit is performed, the latter correction is often introduced to recover on an empirical basis the limitations affecting extrapolation procedures carried out with small- to medium-sized basis sets. Based on the comparison with best-estimated equilibrium structures obtained using the 'gradient' scheme as well as with experiment,[20,29–31,127] the overall conclusion is that the so-called 'cheap' geometry scheme is robust, reliable and accurate, even when dealing with rather flexible molecules like glycine[29] and pyruvic acid.[30] For bond distances, for instance, it is noted that the maximum absolute deviation with respect to CCSD(T)/CBS + CV is smaller than 0.001 Å.

According to Eq. (13) and to the results summarized in Table 1, the evaluation of the rotational constants to be used in the actual prediction of the rotational spectrum involves the determination of the vibration-rotation interaction constants, with the latter requiring in turn the computation of the cubic force field. On the basis of the literature on this topic

TABLE 1 | Statistical Analysis of the Relative Errors (in %) in the Computed Rotational Constants with Respect to Experimentally Determined Equilibrium B^{eq} and Vibrational Ground-State B^0 Values[1]

Computational Approach	$\overline{\Delta}$[2]	$\overline{\Delta}_{abs}$[3]	Δ_{std}[4]
With respect to B^{eq}			
fc-CCSD(T)/cc-pV6Z	–0.277	0.296	0.158
fc-CCSD(T)/CBS	–0.253	0.274	0.141
fc-CCSD(T)/cc-pV6Z + CV	0.041	0.057	0.100
fc-CCSD(T)/cc-pV6Z + CV + ΔT	0.071	0.087	0.110
fc-CCSD(T)/cc-pV6Z + CV + ΔT + ΔQ	–0.027	0.063	0.072
fc-CCSD(T)/CBS + CV + ΔT + ΔQ	–0.003	0.041	0.071
With respect to B^0			
fc-CCSD(T)/CBS	0.380	0.499	0.643
fc-CCSD(T)/CBS + CV	0.690	0.762	0.590
fc-CCSD(T)/CBS + CV + ΔT + ΔQ	0.632	0.710	0.594
fc-CCSD(T)/CBS + CV + ΔT + ΔQ + ΔB_{vib}[5]	0.007	0.057	0.124

[1] Data from Ref 110.
[2] Mean error.
[3] Mean absolute error.
[4] Standard deviation.
[5] Vibrational corrections evaluated using Eq. (13) at the CCSD(T)/cc-pCVQZ level of theory with all electrons correlated.

(see Refs 32,110,123,127,129 and references therein), the level of theory required ranges from DFT in conjunction with double-ζ basis set to CCSD(T) in combination with quadruple-ζ set.

Moving to harmonic force fields, a composite approach similar to the 'cheap' geometry scheme for equilibrium structures is employed to obtain best estimates for the vibrational energies:

$$\omega(\text{best}) = \omega(\text{CCSD(T)/VTZ}) + \Delta\omega(\text{CBS}) + \Delta\omega(\text{CV}) + \Delta\omega(\text{aug}) \quad (23)$$

where ω(CCSD(T)/VTZ) denotes the harmonic wavenumbers at the CCSD(T)/cc-pVTZ level in a normal coordinates representation. The CBS, CV, and aug corrections are defined in the same way as for geometries, with the additional necessary condition being related to the normal modes correspondence for all employed levels of theory. On the basis of the available literature,[29–31,131] this scheme is able to provide harmonic wavenumbers with an accuracy of 1–2 cm^{-1} with respect to CCSD(T)/CBS + CV,[31] with improvements of 5–10 cm^{-1} with respect to CCSD(T)/cc-pVTZ.[29,31,131] An analogous composite scheme has also been derived to determine best estimates for the IR intensities,[29,31,131] I(best), within the double-harmonic approximation. Since extrapolation schemes have not been formulated yet for such a property, Eq. (23) has been reformulated as follows:

$$I(\text{best}) = I(\text{CCSD(T)/VTZ}) + \Delta I(\text{CV}) + \Delta I(\text{QZ-TZ}) + \Delta I(\text{aug}) \quad (24)$$

where ΔI(QZ-TZ) is the correction from the 'MP2/cc-pVQZ - MP2/cc-pVTZ' difference, and the other contributions are defined similarly to vibrational energies.

As a byproduct of the harmonic force fields evaluated at different levels of theory in the frame of the so-called 'cheap' scheme, best estimates for quartic centrifugal-distortion constants can be derived using the same composite scheme defined for IR intensities in Eq. (24). While there is remarkable literature concerning the accuracy and the convergence behavior of computed rotational constants, little has been done by contrast on the centrifugal-distortion constants. In Refs 132, the quartic and sextic centrifugal-distortion constants were evaluated at the HF-SCF, CCSD, and CCSD(T) levels in conjunction with a hierarchical series of basis sets, ranging from triple- to quintuple-ζ quality. With respect to the CCSD(T)/aug-cc-pCVnZ calculations, it is noted that both quartic and sextic centrifugal-distortion constants show a monotonic trend while enlarging the set, thus allowing conclusions to be drawn regarding the convergence to the basis-set limit and the error due to the basis-set truncation. On these grounds, the CCSD(T)/aug-cc-pCV5Z values have a residual basis-set error no larger than 0.2%. By comparison of the constants evaluated at the HF-SCF, CCSD, and CCSD(T) levels of theory, reliable centrifugal-distortion constants can already be obtained at the HF-SCF level, with discrepancies on average of 10–15% with respect to CCSD. Another observation is that the effects of triples are small, the differences between CCSD(T) and CCSD being on average of 1–2%. Therefore, the effect of higher excitations is expected to be almost negligible. Since the CCSD(T) method provides converged results with respect to the truncation of the wavefunction and the composite scheme mentioned above is sufficient to recover the error due to the basis-set truncation, the application of the latter scheme leads to a quantitative estimate of the quartic centrifugal-distortion constants. Due to the very small magnitude of the sextic centrifugal-distortion terms, any level of theory is sufficient to get good predictions.

The evaluation of anharmonic corrections requires some sampling of the potential energy and property surfaces, thus leading to strong limitations in the level of theory affordable. To achieve high accuracy, so-called hybrid QM/QM' approaches need to be employed. These models combine an evaluation of the equilibrium structure, as well as of the harmonic PES and PS, at the highest possible QM level (including composite schemes) with anharmonic corrections computed by means of less expensive QM' techniques. In particular, the combination of CCSD(T) with DFT functionals, thus resulting in a plethora of hybrid CC/DFT approaches, has been well tested for small- to medium-sized closed- and open-shell molecular systems, also including several potential astroCOMs.[16,30,31,62,104,133,134]

The definition of hybrid models requires to evaluate, as a first step, the performance of computationally less-demanding QMs and then to select those suitable for obtaining anharmonic corrections at the desired accuracy. In this respect, it is crucial to assure that these methodologies predict reliable equilibrium structures, harmonic vibrational wavenumbers (ω), normal modes ($\boldsymbol{q}$), and IR intensities (I_{IR}). An appealing factor of the methodologies rooted in the DFT[135] is that they are able to provide results with a reasonably good accuracy, in particular in comparison to the computationally more demanding MP2[128]

method. Among the many methods available, hybrid or double hybrid functionals, like B3LYP[136] and B2PLYP,[137] combined with basis sets of double- and triple-ζ quality, also containing polarization and diffuse functions, are demonstrated to be particularly effective. Nevertheless, it is of crucial importance to verify the accuracy of the DFT equilibrium structures first. In addition to the CCSD(T)/CBS + CV geometries, whose performance has been discussed above, an effective and reliable testing ground is offered by the so-called semiexperimental (SE) equilibrium structures (r_{SE}^{eq}).[138] The latter are based on a combination of experimental ground-state rotational constants and computed vibrational corrections for different isotopic species and permit the determination of structural parameters accurate within 0.001 Å and 0.1° for bond lengths and angles, respectively (see Refs 123,139,140). As an illustration of the accuracy reachable by DFT approaches, Table 2 reports the mean (MAE) and maximum (|MAX|) absolute errors for the bond lengths of a set of small- and medium-sized, semirigid and flexible astroCOMs, including the uracil nucleobase and the glycine aminoacid. With regard to the accessibility of accurate molecular structures, it is worthwhile noting that a database collecting accurate r_{SE}^{eq} geometries for a large number of small- and medium-sized species has been recently setup.[141,145]

Table 2 confirms the high accuracy of the structural parameters obtained from the CCSD(T)/CBS + CV composite approach and the 'cheap' geometry scheme, with average and maximum discrepancies of about 0.001 and 0.003–0.004 Å, respectively. In particular, the latter model represents a significant improvement over CCSD(T)/cc-pVTZ, with MAE and |MAX| smaller by about 70%, at a limited additional cost due to MP2 computations. The high accuracy of the so-defined 'cheap' equilibrium structures is particularly promising for the astrochemical detection of larger astroCOMs, also including small biomolecules. Concerning less expensive QM models, which can be employed for the generation of the anharmonic PES and PS for molecular systems composed of dozens of atoms, it is evident that the double-hybrid B2PLYP structures are on average slightly better than their MP2 counterparts, at a comparable computational cost.

As a matter of fact, benchmark studies suggest that for larger systems, whenever the evaluation of the harmonic PES by means of composite schemes becomes prohibitively expensive, the B2PLYP functional in conjunction with basis sets of at least triple-ζ quality provides an effective route for both rotational and vibrational spectroscopy investigations.[30,31,62,134,142,146] In particular, for several astroCOMs, it has been shown that vibrational wavenumbers in agreement with experiment within 6–12 cm^{-1} can be obtained from anharmonic GVPT2 calculations based on B2PLYP/aug-cc-pVTZ harmonic PESs,[31,134,144,146,147] to be compared with an accuracy of 4–10 cm^{-1} obtained when using harmonic PESs of CCSD(T)/CBS + CV quality.[31,133,134,146,147] Concerning IR intensities, the B2PLYP/aug-cc-pVTZ results agree with the best-estimated values within 1–2 km mol^{-1}, thus showing the same accuracy as MP2 computations.[31]

The overall good accuracy demonstrated by B2PLYP in the description of the harmonic PESs and PSs fully justifies its use in the evaluation of anharmonic contributions. For fundamental bands, the anharmonic corrections on the wavenumbers agree within 2–7 cm^{-1} with those obtained at the CCSD(T) level, and within 0.5 km mol^{-1} for the IR intensities.[31,146] Therefore, hybrid CC/DFT models with anharmonic corrections at the B2PLYP/aug-cc-pVTZ level give highly accurate results for both vibrational wavenumbers and IR intensities. In particular, this leads for the latter to an agreement within 1 km mol^{-1} with experimental integrated cross sections, which means an error smaller than 5 and 10% for the strongest and weakest signals, respectively.[131,147] Concerning line positions, it should be noted that the only large discrepancies noted, of order of 20 cm^{-1}, involve intramolecular hydrogen bonds, as for instance the $\nu(O\text{-}H)_{HB}$ band of the *Tc* – pyruvic acid.[30] However, even in these cases, the discrepancies of B2PLYP anharmonic wavenumbers with respect to experiment can be entirely related to the harmonic part, at least for the fundamental transitions.[30]

Finally, we can conclude that the least expensive B3LYP model clearly does not provide the accuracy required for the prediction of equilibrium structures and properties in the field of Astrochemistry, with MAEs an order of magnitude larger than those obtainable with the best theoretical approaches. This has also an impact on the harmonic frequencies that therefore show too large errors.[62,146] However, it should be noted that, among the various DFT models, the B3LYP functional still represents a reliable and accurate approach for the evaluation of anharmonic contributions to be coupled to higher-level methods, provided that the normal modes are sufficiently similar. Extensive benchmark studies have shown that B3LYP/SNSD computations can be applied to evaluate accurate vibrational corrections to the rotational constants[32,141] and anharmonic corrections to vibrational wavenumbers and IR intensities.[29,31,62,147] By

TABLE 2 | Accuracy of Equilibrium Bond Lengths Computed by Different quantum-mechanical (QM) Methods[1]

astroCOM	B3LYP[2]	B2PLYP[3]	MP2[3]	CCSD(T)[4]	'cheap'[5]	bestCC[6]
			MAE wrt r_{SE}^{eq}			
Oxirane	0.0059	0.0024	0.0035	0.0048	0.0014	0.0008
Methyloxirane	0.0068	0.0020	0.0026	0.0035	0.0011	0.0009
Acrolein	0.0053	0.0013	0.0022	0.0040	—	0.0006
Pyruvic acid	0.0074	0.0038	0.0048	0.0053	0.0015	0.0011
Pyrimidine	0.0054	0.0008	0.0024	0.0043	0.0006	0.0006
Glycine	0.0075	0.0033	0.0035	0.0045	0.0009	0.0010
Uracile	0.0063	0.0026	0.0041	0.0049	0.0012	—
All	0.0064	0.0023	0.0033	0.0045	0.0011	0.0008
			|MAX| wrt r_{SE}^{eq}			
Oxirane	0.007	0.006	0.009	0.007	0.003	0.001
Methyloxirane	0.008	0.007	0.009	0.005	0.003	0.002
Acrolein	0.009	0.004	0.009	0.007	—	0.002
Pyruvic acid	0.013	0.007	0.010	0.007	0.003	0.003
Pyrimidine	0.007	0.001	0.004	0.007	0.001	0.001
Glycine	0.013	0.008	0.008	0.010	0.003	0.004
Uracile	0.013	0.008	0.008	0.008	0.003	—
All	0.013	0.008	0.010	0.010	0.003	0.004

[1] Mean (MAE) and maximum (|MAX|) absolute deviations (in Å) with respect to the semiexperimental equilibrium structure for oxirane,[20,31] methyloxirane,[31] *trans*- and *cis*-acrolein,[134,141] *Tc*-pyruvic acid,[30] pyrimidine,[141,142] Ip/ttt and IIn/ccc glycine conformers,[29,122,143] and uracile,[127,133,144] complemented by data from this work.
[2] Computed with the SNSD[62] basis set.
[3] Computed with the aug-cc-pVTZ basis set.
[4] Computed with the cc-pVTZ basis set.
[5] Obtained by means of the 'cheap' geometry scheme, for details, see text.
[6] CCSD(T)/CBS + CV equilibrium structure (see text) obtained using the cc-pVTZ and cc-pVQZ basis sets for the complete basis set (CBS) extrapolation and the cc-pCVTZ set for the core-correlation correction.

contrast, many more recent functionals show significantly larger discrepancies with respect to experiment for both harmonic frequencies and anharmonic corrections.[62,146] Thus, the use of newly-developed DFT models in the field of Astrochemistry needs an extensive validation first.[98]

While B3LYP molecular structures are not sufficiently accurate to be used in spectroscopic application, it has been shown that combining B3LYP/SNSD structures and thermodynamic properties with CCSD(T)/CBS + CV electronic energies is a reliable approach to assess the population of conformers.[29] In more details, it is apparent that relative electronic energies computed at the best theoretical and B3LYP/SNSD equilibrium structures usually differ by less than 0.1 kJ mol^{-1}. Thus, the B3LYP/SNSD model represents an effective route for extensive conformational searches that, once followed by accurate estimates of the electronic energies, allows identifying the most stable conformers of astroCOMs on which highly accurate theoretical investigations should be focused.

SPECTROSCOPY OF ASTROCOMS: OXIRANE AS A TEST CASE

Starting from its detection in the ISM[22] as one of the first cyclic molecules, the potential role in Astrochemistry of oxirane has been addressed in several publications (see Refs 16,20,148–150), with special reference to Titan's (the largest moon of Saturn) atmosphere. Raulin and coworkers[148] demonstrated that experiments designed to simulate the upper atmosphere of Titan, i.e., a high voltage applied to a mixture containing methane (CH_4, ~2%), nitrogen (98% N_2), and traces of oxygen (0.01% CO) at low temperature (100–150 K), can lead to the production of oxirane. Furthermore, Bernstein and Lynch demonstrated a close correlation between the IR spectra of oxirane, among others, and the major unidentified infrared bands (UIRs).[151] The relevance of the oxiranes' family is also pointed out by the recent, first detection of a chiral molecule, methyloxirane, in a cold, extended molecular shell around the embedded, massive protostellar clusters in the Sagittarius B2

star-forming region.[19] In view of its broad astrochemical relevance and the fact that its spectroscopy has been very well characterized from a computational and experimental point of view, we use oxirane as a test case to introduce and discuss the computational approach described in the previous section.

Definition of the Protocol

The equilibrium rotational constants have been directly derived from the equilibrium geometry obtained by means of the CCSD(T)/CBS + CV 'gradient' scheme (see Eq. (21)) in conjunction with large basis sets (cc-pVQZ and cc-pV5Z for the extrapolation to the CBS limit and cc-pCVQZ for the CV contribution). To predict the ground-state rotational constants, these best-estimated equilibrium rotational constants have been subsequently augmented by vibrational and electronic corrections at the CCSD(T)/cc-pVQZ and CCSD(T)/aug-cc-pVQZ levels, respectively. The latter are due to the electronic-distribution contribution to the moments of inertia and are thus connected to the rotational g-factor (see Refs 123). Quartic and sextic centrifugal-distortion constants have been obtained by means of composite schemes, the same one being employed for the quartic terms and best-estimated harmonic wavenumbers (in a normal coordinate representation). In detail, the CCSD(T)/CBS + CV + aug scheme has been used, with the extrapolation to the CBS limit based on results at the CCSD(T)/cc-pVTZ and CCSD(T)/cc-pVTQZ levels, the CV contribution evaluated at the CCSD(T)/cc-pCVTZ level, and the 'aug' correction determined by comparison of CCSD(T)/aug-cc-pVTZ and CCSD(T)/cc-pVTZ values. For sextics, a composite approach analogous to the previous one has been employed, however, neglecting the 'aug' contribution.

The anharmonic vibrational wavenumbers and IR intensities have been computed using the GVPT2 model applied to hybrid 'CC(Best)/CC' anharmonic force fields: the harmonic force field obtained at the CCSD(T)/CBS + CV + aug has been combined with anharmonic terms at either the CCSD(T)/cc-pVTZ or CCSD(T)/cc-pVQZ level. For an exhaustive account, the reader is referred to Refs 20. For comparison purposes, the harmonic force field from the 'cheap' scheme has also been considered.[152] The anharmonic PESs and PSs have been computed employing different QM methods: B3LYP/SNSD, B2PLYP/aug-cc-pVTZ, CCSD(T)/cc-pVTZ, and CCSD(T)/cc-pVQZ.

Rotational Spectroscopy

The rotational spectroscopy parameters of oxirane computed using the protocol described above are summarized in Table 3, where they are compared to the available experimental data. We note a very good agreement between our best estimates and experiment, with discrepancies on the order of 0.1, 2–3%, and 3–4% for rotational, quartic, and sextic centrifugal-distortion constants, respectively.

As mentioned in the *Introduction*, the target here are the spectroscopic signatures. Our best-estimated parameters (first column of Table 3) lead to the prediction of rotational transitions with a relative accuracy better than 0.1% in the centimeter/millimeter-wave region, with this upper limit increasing up to 0.15% in the FIR region. This means that our computed parameters can predict rotational frequencies of 100 GHz and 2 THz with an uncertainty, in the worst case, of 100 MHz and 3 GHz, respectively. Figure 2 shows two portions, at ~85 and ~104 GHz, of the rotational spectrum of oxirane. Comparison with experiment confirms the expected accuracy: the discrepancies in relative terms range from 0.002 ($J = 6_{2,\,4}$–$6_{1,\,5}$) to 0.09% ($J = 2_{2,\,0}$–$1_{1,\,1}$). To further improve the predictive capability of our computational protocol, a scaling procedure can be applied:

$$X_{\mathrm{scal}}^{\mathrm{oxi}} = X_{\mathrm{calc}}^{\mathrm{oxi}} \times \left(X_{\mathrm{exp}}^{\mathrm{ref}} / X_{\mathrm{calc}}^{\mathrm{ref}} \right) \qquad (25)$$

where X denotes a generic spectroscopic parameter. The superscripts 'oxi' and 'ref' refer to oxirane and the reference compound, respectively; 'scal,' 'exp,' and 'calc' denote the scaled, experimental, and quantum-chemically calculated values for X. The idea at the basis of this empirical refinement is that the discrepancies affecting the computed spectroscopic constants are in some way systematic and thus, chosen a reference species that shares some similarity in the electronic structure with oxirane, a sort of scaling factor can be derived. We avoid the definition of a unique scaling factor, but instead we obtain one for each parameter, even if we can point out that the resulting scaling factors are generally very similar to one another. The empirical scaling has demonstrated to be extremely effective if the reference molecule is an isotopic species, as shown in Refs 20 for monodeuterated oxirane (with the main isotopic species used as reference compound). However, in the present case, for demonstrative purposes, methyloxirane has been chosen as the reference molecule. For both oxirane and methyloxirane, the equilibrium rotational constants have been determined at the CCSD(T)/CBS + CV level using the cc-pVTZ and cc-

TABLE 3 | Ground-State Spectroscopic Parameters of Oxirane

Parameter		Best Estimate[1]	Calculated[2]	Scaled[3]	Experiment[4]
A	(MHz)	25,528.216	25,540.56	25,491.12	25,483.86060(96)
B	(MHz)	22,121.162	22,135.67	22,119.82	22,120.87122(88)
C	(MHz)	14,110.762	14,118.44	14,101.74	14,097.82440(55)
Δ_J	(kHz)	20.537	20.33	20.11	20.68572(77)
Δ_{JK}	(kHz)	21.630	19.62	21.49	20.91000(216)
Δ_K	(kHz)	26.725	27.09	27.22	27.59143(275)
δ_J	(kHz)	6.104	6.12	6.19	6.210757(211)
δ_K	(kHz)	17.654	17.14	17.38	18.10778(120)

[1] Equilibrium rotational constants corresponding to a best-estimated CCSD(T)/CBS + CV equilibrium structure obtained using the cc-pVQZ and cc-pV5Z basis sets for the CBS extrapolation and the cc-pCVQZ set for the core-correlation correction.Corrections to rotational constants: Vibrational at the CCSD(T)/cc-pVQZ level and electronic at the CCSD(T)/aug-cc-pVQZ level.Best-estimated quartic centrifugal-distortion constants obtained with the CCSD(T)/CBS + CV + aug scheme.For details, see Ref 20.
[2] Equilibrium rotational constants corresponding to a CCSD(T)/CBS + CV equilibrium structure obtained using the cc-pVTZ and cc-pVQZ basis sets for the complete basis set (CBS) extrapolation and the cc-pCVTZ set for the core-correlation correction.Vibrational corrections to rotational constants at the B3LYP/SNSD level.Quartic centrifugal-distortion constants at the CCSD(T)/cc-pCVTZ level (all electron).
[3] Spectroscopic parameters evaluated according to footnote 2 scaled using those of methyloxirane computed at the same level and the corresponding experimental data.[153]
[4] Experiment: Ref 154.

pVQZ basis sets for the CBS extrapolation and the cc-pCVTZ set for the core-correlation correction, successively augmented by vibrational corrections at the B3LYP/SNSD level.[31] The parameters of oxirane have been scaled according to Eq. (25), using the experimental data recently reported for methyloxirane.[153] The calculated and scaled spectroscopic constants (second and third column of Table 3, respectively) are compared to experiment (fourth column). A significant improvement is noted; for rotational constants, for example, the discrepancy is reduced to 0.03% or even lower. This improvement in turn leads to better predictions of the rotational transitions with respect to the best-estimated level, as seen in panel *b*) of Figure 2, with deviations below 0.01–0.02%. We finally note that the empirical scaling permits the determination of rotational-parameter values with spectroscopic accuracy, which means in this context that the predicted results are within 0.01–0.03% from experiment.

Vibrational Spectroscopy

The GVPT2 fundamental wavenumbers and IR intensities of oxirane computed using the protocol described above are compared in Table 4 with the most accurate gas-phase experimental results. Notably, a very good agreement with experiment is achieved, with mean absolute errors and maximum deviations of about 5.5–7.5 and 9–13 cm^{-1}, respectively, for all hybrid models when the harmonic part is evaluated by means of a composite scheme accounting for extrapolation to the CBS limit and core correlation effects (either 'bestCC,' i.e., CCSD(T)/CBS + CV + aug, or the 'cheap' scheme). We note that when the 'bestCC' harmonic part is employed, the MAE and |MAX| values are within 5.3–5.6 cm^{-1} and 9–11 cm^{-1}, respectively, for all hybrid models, regardless of the way the anharmonic correction has been evaluated, from expensive CCSD(T)/cc-pVQZ computations or from B3LYP/SNSD. Based on the results presented in Table 4, but also on several studies available on this topic (see Refs 30,131,147), CC/QM' hybrid force fields, where CC stands for a CCSD(T)-based composite approach, are able to predict transition wavenumbers with an accuracy of about 5–10 and 10–20 cm^{-1} for fundamental and nonfundamental bands, respectively. The latter error estimate for overtones and combination bands is in line with the discrepancy between the theoretical 'bestCC'/CCSD(T)/cc-pVQZ (2922 cm^{-1}) and experimental (2931 cm^{-1}) wavenumbers for the intense band corresponding to the combination $\upsilon_2 + \upsilon_{10}$.[20] Concerning IR intensities, we note in all cases a good qualitative agreement, while a more quantitative analysis is precluded due to large error bars often affecting experimental data because of the limited resolution.[158] Nevertheless, when high-resolution data are available, namely for υ_2, υ_5, and υ_{10},[156,160] theoretical results agree well within 10%. Furthermore, we note that the reliability of our computed CC/QM' fully anharmonic IR intensities has been recently demonstrated not only for fundamentals, but also for overtones and combination bands.[131,147] The overall conclusion is that the high accuracy of GVPT2 CC/QM' results allow an accurate and complete

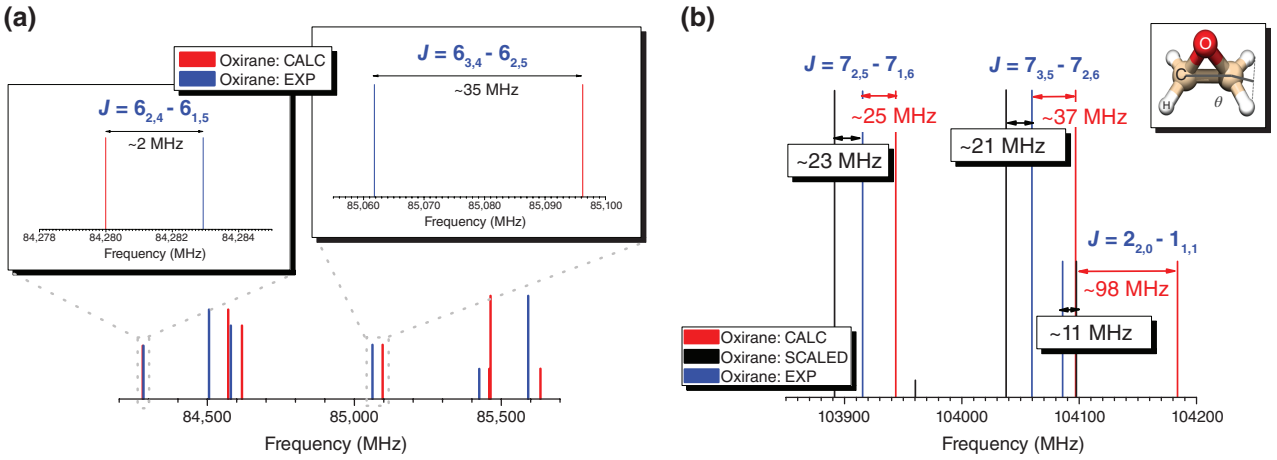

FIGURE 2 | Comparison of the best-estimated (see footnote 1 of Table 3, in red), scaled (in black) and experimental (Ref 154, in blue) rotational spectrum of oxirane in the (a) ~85 GHz and (b) ~104 GHz frequency regions.

characterization of the IR spectrum of oxirane in terms of band positions and intensities, including overtones and combination bands. The theoretical predictions of all intense transitions, from mid IR (MIR) to near-IR (NIR), represent a valuable support for the detection of oxirane and other astroCOMs in new space environments through their vibrational signatures. In particular, the 'cheap' composite scheme can be effectively applied to the investigation of astroCOMs up to about a dozen of nonhydrogen atoms. We also note an overall good quality of the B2PLYP/aug-cc-pVTZ computations, with mean absolute errors below 10 cm^{-1} and maximum discrepancies below 20 cm^{-1}. This finding is of interest for astrochemical studies of significantly larger systems, for which harmonic PES computations at the CCSD(T)/cc-pVTZ level are not feasible.

As an example, we present a comparison between the simulated emission spectra of oxirane in the 3–13 μm range (800–6000 cm^{-1})[20] and the astronomical observations of the planetary nebula NGC 7027, as reported in a uniform database (2.4- to 45.4-μm spectra) from the Infrared Space Observatory Short Wavelength Spectrometer (ISO-SWS).[161] Figure 3 shows selected parts of the spectra, in the 3.2–3.8 and 10.5–13.0 μm ranges, along with all identified line fluxes[162] marked by vertical gray lines, thus clearly showing that several, still unidentified IR (UIR) transitions could be assigned. From Figure 3, we note that the group of oxirane transitions related to the CH_2 stretching fundamental vibrations match well the observed UIR feature at 3.3 μm; similarly the one at 3.4 μm is well represented by the strong combination band $\upsilon_2 + \upsilon_{10}$. In particular, a reliable prediction of the latter requires fully anharmonic computations in order to assess the band position and absolute intensity. Nevertheless, this good match cannot be conclusive for the detection of oxirane because the broad features in the ISO-SWS database are most likely resulting from CH stretching vibrations of several astroCOMs. In this respect, a good agreement between our best-estimated spectra and less computationally demanding models (in particular based on B2PLYP) in reproducing the main spectral features opens a path to reliable simulations of more complex, aromatic, and aliphatic molecules suggested to be present in circumstellar and interstellar nebulae.[163] More characteristic of oxirane is its most intense band at 11.45 μm (873 cm^{-1}), which is related to the ring deformation, and for which the good match with the 11.2–11.3 μm UIR feature provides a more plausible support to oxirane detection. This band can also be chosen to distinguish between oxirane and methyloxirane, which shows weaker features at 10.53 and 12.05 μm (950 and 830 cm^{-1}) that are related to the ring deformation and the ring C-C stretching, respectively.[31] Unfortunately, this band cannot be used for the possible identification of oxirane in Titan's atmosphere, as the IR spectra recorded by Cassini's (CIRS) instrument over the 10–1500 cm^{-1} range show a strong absorption at 11.5–12.5 μm (800–860 cm^{-1}) due to the ethane υ_9 band, thus hiding any close-lying transitions.

CHALLENGES IN COMPUTATIONAL SPECTROSCOPY OF ASTROCOMS

Spectral surveys, which consist of a series of spectra covering, at millimeter/submillimeter wavelengths,

TABLE 4 | Theoretical Predictions of GVPT2 Wavenumbers (ν / cm^{-1}) and Infrared Intensities (I_{IR} / km mol^{-1}) for Oxirane Fundamental Transitions, Compared to Experiment

		B2PLYP[1]		'cheap'[2]				bestCC[3]						Experiment			
				B2PLYP[1]		CCSD(T)[4]		B3LYP[5]		B2PLYP[1]		CCSD(T)[6]					
Mode	Symm.	ν	I_{IR}	ν	I_{IR}	ν	I_{IR}	ν	I_{IR}	ν	I_{IR}	ν	I_{IR}	ν	I_{IR}[7]	Ref	Assignment
υ_1	A1	3031	9.5	3025	11.3	3018	13.8	3027	16.4	3024	15.9	3021	15.9	3018		[155]	CH_2 sym stretch
υ_2	A1	1500	1.2	1489	1.1	1487	1.2	1492	0.9	1489	1.1	1490	1.2	1498	0.92(0.06)	[156,157]	CH_2 scissor
υ_3	A1	1272	14.2	1265	14.0	1264	13.8	1270	14.2	1268	13.8	1266	13.6	1270	13.16(0.45)	[157–159]	Ring breathing
υ_4	A1	1124	0.4	1118	0.6	1115	0.4	1120	0.2	1119	0.3	1115	0.2				CH_2 wagging
υ_5	A1	866	68.7	869	72.7	869	72.7	876	72.0	875	68.7	873	68.9	877	64.76(3.6)[8]	[157,160]	Ring deformation
υ_6	A2	3057	0.0	3061	0.0	3058	0.0	3064	0.0	3062	0.0	3065	0.0				CH_2 asym stretch
υ_7	A2	1163	0.0	1155	0.0	1156	0.0	1157	0.0	1156	0.0	1160	0.0				CH_2 rocking
υ_8	A2	1028	0.0	1025	0.0	1019	0.0	1027	0.0	1026	0.0	1027	0.0				CH_2 twisting
υ_9	B1	3026	23.2	3016	19.1	3009	29.5	3017	30.2	3015	31.4	3009	31.4	3007	44.31(5.95)	[155,158]	CH_2 asym stetch
υ_{10}	B1	1478	0.1	1464	0.4	1462	0.3	1465	0.1	1463	0.1	1461	0.1	1471	0.25(0.06)	[156,157]	CH_2 scissor
υ_{11}	B1	1147	0.2	1145	0.1	1150	0.2	1145	0.2	1144	0.3	1154	0.2				CH_2 wagging
υ_{12}	B1	809	10.4	809	9.1	809	8.6	818	9.3	817	8.8	816	8.3	822	8.56(0.80)	[157,158]	Ring deformation
υ_{13}	B2	3071	44.3	3074	32.3	3071	31.9	3077	32.0	3075	35.0	3076	34.2	3066	36.24(4.69)	[155,158]	CH_2 asym stretch
υ_{14}	B2	1149	3.6	1143	4.0	1141	4.2	1146	4.3	1145	4.1	1145	4.1				CH_2 twisting
υ_{15}	B2	812	0.1	807	0.4	806	0.5	807	0.3	807	0.2	810	0.3	808	0.21(0.21)	[157,158]	CH_2 rocking
	MAE[9]	8.4		7.3		6.2		5.3		5.6		5.4					
	| MAX |[9]	18.9		12.8		12.9		11.0		9.0		10.0					

[1] Computed with the aug-cc-pVTZ basis set.
[2] Harmonic wavenumbers and infrared (IR) intensities obtained by means of the 'cheap' composite scheme. For details, see Ref 152.
[3] CCSD(T)/CBS + CV + aug harmonic wavenumbers and IR intensities (for details, see text and Ref 20).
[4] Computed with the cc-pVTZ basis set.
[5] Computed with the SNSD basis set.
[6] Computed with the cc-pVQZ basis set.
[7] Numbers given in parenthesis are the experimental errors.
[8] Total intensity in the spectral region 750–950 cm^{-1} corresponding to the υ_5, υ_{12}, and υ_{15} fundamental transitions. For details, see Ref 160
[9] Mean absolute error (MAE) and maximum absolute deviations (|MAX|) with respect to experimental wavenumbers.

several dozens of GHz with a uniform sensitivity, are the ideal mean to obtain a complete census of the species emitting in the investigated astronomical object. The first step of their analysis thus consists in identifying the various lines, with the main difficulty being related to those molecules responsible for hundreds of them. These are species that are characterized by LAM(s) that often occur at low wavenumbers. Typical examples are methanol, methyl formate, or dimethyl ether, and the large number of lines is usually due to rotational transitions in low-frequency vibrational modes (like those associated to the methyl rotor). In addition to the difficulty of astronomical detection and identification, these molecules represent a major challenge for molecular spectroscopy and, in particular, for computational spectroscopy.

Another important issue is the identification of conformers and their relative abundances, which might become crucial when astronomical observations involve the hotter regions of the ISM, like star-forming sources known as 'hot cores.' Among the astroCOMs, in relation to the issue of the origin of life, particular interest is devoted to those showing a prebiotic character. These species are usually flexible systems and therefore their conformational equilibrium needs to be taken into account and precisely investigated. Inaccurate or wrong evaluations of the relative conformational energies may give misleading results and conclusions.

Large Amplitude Motion

A large number of unidentified lines, especially in spectra of the hot cores associated with star formation, are due to rotational transitions in the low-lying excited vibrational states of a relatively small number of molecules, denoted as 'astrophysical weeds' (see Refs 164 and references therein). From a computational point of view, it is necessary to characterize the rotational spectra in the vibrational ground state and in the low-lying vibrational states, and understand how they are affected by LAM(s).

The recent computational spectroscopic characterization of acetyl cyanide (CH_3COCN) and its enolic species[165] provides the opportunity to point out the accuracy obtainable in the computation of the spectroscopic parameters of interest. Acetyl cyanide belongs to those medium-sized molecules (6–10 atoms), detected or expected to exist in the ISM, that show a potential prebiotic character because present in plausible chemical routes to simple biomolecules, like amino acids or simple peptides. Therefore, a lot of effort has been put in the identification of these compounds, their precursors, or their fragments.

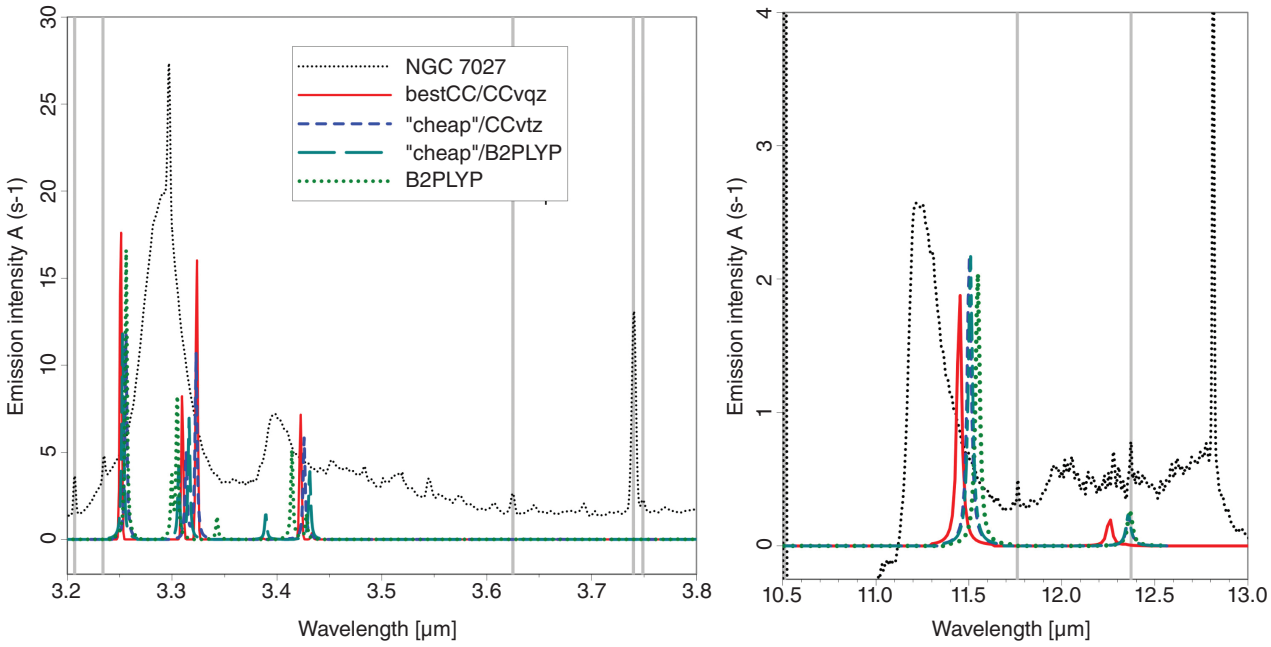

FIGURE 3 | Comparison between the simulated (color) spectra of oxirane and the observed (black) emission spectra of planetary nebula NGC 7027 (Sloan et al.[161]). Selected wavelength ranges: (a) the 3.2–3.8 μm and (b) 10.5–13.0 μm. The observed identified line fluxes reported by Salas et al.[162] are marked by the gray lines. Computations with hybrid models are denoted as QM/QM′, with CCvxz (x = t,q) standing for CCSD(T)/cc-pVXZ. Theoretical spectra have been convoluted with a Lorentzian function with half-width at half-maximum of 1 cm^{-1}.

Although acetyl cyanide has not been detected yet, it is expected to be present in the ISM. Its electronic ground state has been already well characterized experimentally, thus giving us the opportunity to demonstrate how highly accurate QM approaches are able to deal with the challenges raised by hindered methyl rotor in rotational spectroscopy.

The methyl group of acetyl cyanide is involved in a torsional vibrational motion rather well separated from the other modes of the systems. As a result, the impact of this motion on the rotational spectrum can be evaluated by mean of a one dimensional-model along the torsional angle α (see Figure 4) representing the internal rotation of the -CH_3 group relative to the -COCN frame, which leads to three equivalent configurations. Therefore, the potential energy function with respect to α is periodic and can be modeled by the expression:

$$V(\alpha) = \frac{V_3}{2}[1 - \cos(3\alpha)] \qquad (26)$$

In the limit of an infinite barrier, each torsional state v is threefold degenerate. For a finite barrier, the tunneling effect leads to a splitting of this threefold degeneracy (because of the probability of tunneling through the barrier) into two levels, a nondegenerate A level and a doubly-degenerate E level (see Figure 4). As a consequence, in the rotational spectrum, we observe rotational transitions in the A and E torsional sublevels for each vibrational state; in other words, the rotational spectrum of acetyl cyanide in its vibrational ground state results from the overlap of the rotational spectrum of the A state and that of the E state. Therefore, to predict the overall spectrum the rotational constants for both A and E sublevels are needed.

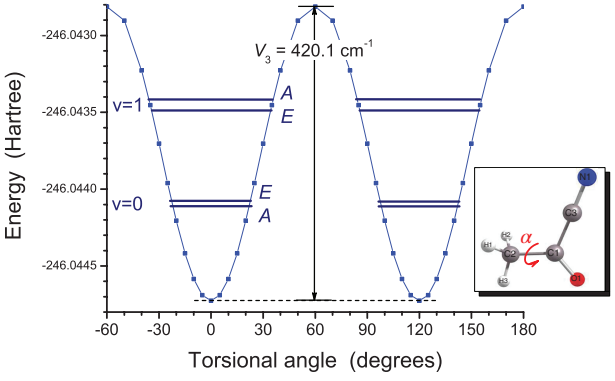

FIGURE 4 | The potential energy profile of acetyl cyanide along the torsional angle (see, the inset) evaluated at the CCSD(T)/CBS + CV level using CCSD(T)/cc-pVTZ optimized geometries.

In Refs 165, the CCSD(T)/CBS + CV 'gradient' scheme has been employed to accurately predict the equilibrium rotational constants, while the vibrational corrections have been evaluated using the VPT2 approach with a cubic force field computed at the MP2/aug-cc-pVTZ level, which also provided the sextic centrifugal-distortion constants. The 'cheap' geometry scheme has been used instead to generate the harmonic force field, which allowed in turn the evaluation of the quartic centrifugal-distortion terms. To predict the rotational constants of the E state, it is necessary to calculate the V_3 barrier. For this purpose, the potential energy function along the torsional angle has been determined at the CCSD(T)/cc-pVTZ level by carrying out geometry optimizations with the α value kept fixed (also known as a relaxed scan), as shown in Figure 4. In a subsequent step, the energy evaluation has been improved by single-point calculations at the CCSD(T)/CBS + CV level on the CCSD(T)/cc-pVTZ optimized structures, thus leading to a V_3 value of 420.1 cm^{-1}, in good agreement with the experimental value (V_3 = 404.867(90) cm^{-1}).[166] The computed spectroscopic parameters are collected in Table 5, where they are compared to their experimental counterparts. Despite a slight overestimation of the splitting between A and E rotational constants, the overall accuracy is very satisfactory. In Table 5, the prediction of the rotational constants for the lowest vibrational states (v_{18} = 1 and v_{12} = 1) together with the available experimental data is also reported. Making use of Eq. (25), the computed data have also been scaled based on the experimental values for the vibrational ground state. For all rotational constants, the discrepancies between experiment and theory, in relative terms, are well below 0.1%, a value which can be further improved (to ~0.03%) by applying an effective empirical strategy such as the scaling procedure. In Refs 165, a comparison between the computed and experimental centrifugal-distortion constants is also provided. For the best-estimated quartic centrifugal-distortion constants, the average discrepancy with respect to experiment is about 2.7%, which can be viewed as a very good result because of the presence of a LAM and the smallness of these constants. The sextic centrifugal-distortion constants are extremely small, the largest ones being only a few tenths of Hz. Therefore, an average discrepancy in relative terms with respect to experiment of 16% can be considered a good outcome.

The large amplitude vibrations cannot be accurately described by perturbative approaches, and require an expansion of the PES beyond the quartic order. A possible solution, albeit limited to small

molecules (i.e., less than ten vibrational degrees of freedom), is to carry out fully variational computations of the rovibrational energy levels.[35–37,167] However, more effective models are required for larger systems, like the astroCOMs. In this respect, it is convenient to separate the degrees of freedom related to small-amplitude vibrations and LAMs. A major difficulty actually lies in a proper separation of the two sets of vibrations because the mode coupling can be significant, in particular at the anharmonic level. A first step is to ensure that such couplings are minimized, which can be done through different strategies, for instance by localizing the normal modes[168–170] or by using suitable sets of coordinates, like the internal ones.[77,171] Depending on the level of sophistication sought and on the complexity and cost of the calculations, LAMs can be completely isolated, by assuming they are uncoupled, or connected to the rest of the system using *ad hoc* schemes to describe the mixing. Robust strategies have been proposed at the harmonic level for both vibrational and vibrationally resolved electronic spectroscopies, by treating the LAM separately or with hybrid schemes,[172] like those based on the reaction path/surface Hamiltonian.[173–176] Their extension to anharmonic force fields[176,177] is less straightforward and requires additional considerations, beyond the scope of the present review. Still, we should note that even for molecules showing both LAMs and small-amplitude vibrations, standard VPT2 computations based on Cartesian-based normal coordinates for the whole system allow mapping all molecular vibrations and represents a feasible route, for instance, to check whether there are any Fermi interactions between large- and small- amplitude vibrations.[178] This can then represent a first step in establishing a suitable strategy to build a model able to describe accurately both large and small amplitude motions.

An interesting example in the field of Astrochemistry[24] is represented by ethyl mercaptan[178] (EtSH), with the *gauche* conformer only slightly more stable than the *trans* one with an energy difference of 162 cm^{-1}. The conformational flexibility of this molecule is related to the H-S-C-C torsional angle (see Figure 1), which leads to a potential energy profile with barriers within 350–500 cm^{-1}. In EtSH, there is a second LAM, which corresponds to the internal rotation of the methyl group and is characterized by a significantly larger barrier of about 1200 cm^{-1}. Both conformers show dipole moments of the same order of magnitude (about 1.8 Debye), which render possible their detection in the ISM by means of radioastronomical observations in either millimeter-/submillimeter-wave or IR ranges. In Refs 178, in order to provide the required spectroscopic characterization, the H-S-C-C torsional motion and the internal rotation of the methyl group have been excluded from the perturbative description and treated variationally. For this purpose, a two-dimensional PES has been computed at the CCSD(T)/aug-cc-pVTZ level of theory, then the couplings with other vibrational degrees of freedom have been taken into account through an effective correction of their contribution to the ZPVE. The reader is referred to Refs 178 for all details. These computations allowed the accurate determination of the torsional energy levels, including the tunneling splitting observed for the *gauche* conformer. The results are summarized in Table 6, which highlights the large differences between the *gauche* and *trans* ethyl mercaptan spectral features in the FIR region. In particular, the fundamental transitions for the SH and CH torsions of *gauche*-EtSH are localized at 188.87 cm^{-1} with a splitting of 1.47 cm^{-1} and at 254.06 cm^{-1} with a splitting of 0.02 cm^{-1}, respectively. They clearly do not superimpose with those of *trans*-EtSH, which are shifted by 32 and 9 cm^{-1}, respectively. In Table 6, the variational computations can be compared with the GVPT2 results, thus showing that the perturbative treatment provides reasonable frequencies for the CH torsion of both conformers and for the SH torsion of *gauche*-EtSH. This is not the case for the SH torsion of *trans*-EtSH, for which the first excited energy level lies above the torsional barrier.[178]

The problem of a reliable treatment of large-amplitude modes is not only related to their direct detection in the FIR region, but also to the coupling with other vibrations that can be observed in the MIR range. In this respect, the LAM can contaminate significantly the VPT2 treatment, thus leading to large errors even for the intense, high-frequency vibrations. This issue can be overcome by employing reduced-dimensionality perturbative models, where LAMs are excluded from the VPT2 treatment. The efficiency of such an approach is displayed in Table 7, which collects some examples for the *gauche* conformer of EtSH, discussed above, and the nucleobase cytosine. For the latter, the LAM is the out-of-plane wagging vibration of the NH_2 group (see Figure 1). The coupling of the torsional and wagging LAMs with the H-X (X = C, S, N) stretching vibrations results in an incorrect prediction of the latter by means of GVPT2. At variance, in the reduced-dimensionality GVPT2 models (i.e., the so-called 'SkipPT2' approach), the LAMs and all related cubic and quartic force constants are excluded from the perturbative treatment. As evident from Table 7, this procedure leads to the accurate prediction of the

TABLE 5 | Computed and Experimental Rotational Constants (MHz) of Acetyl Cyanide for the Vibrational Ground State and for the $v_{18} = 1$ and $v_{12} = 1$ Vibrational States

	A State		*E* State		
Parameter	Best theo.[1]	Experiment[2]	Best theo.[1]	Experiment[2]	Scaled[3]
Ground state					
A_0 / MHz	10,193.6	10,185.37774(26)	10,193.0	10,185.13561(34)	
B_0 / MHz	4157.3	4157.48341(11)	4157.0	4157.37176(10)	
C_0 / MHz	3003.2	3002.76275(11)	3003.2	3002.76390(12)	
D_J / kHz	0.790	0.816733(84)			
D_{JK} / kHz	17.916	17.80532(26)			
D_K / kHz	−7.029	−6.6543(10)			
d_J / kHz	0.256	0.266340(26)			
d_K / kHz	10.382	10.42700(48)			
H_J / Hz	3.410×10^{-4}	$4.51(21) \times 10^{-4}$			
H_{JK} / Hz	0.202	0.17658(16)			
H_{KJ} / Hz	−0.437	−0.37141(51)			
H_K / Hz	0.285	0.2519[10]			
h_J / Hz	1.714×10^{-4}	$2.183(54) \times 10^{-4}$			
h_{JK} / Hz	0.104	0.09265(15)			
h_K / Hz	0.479	0.4374(10)			
$v_{18} = 1$ (126.06 cm^{-1})					
A_0 / MHz	10,195.3	10,191.8472(22)			10,187.1
B_0 / MHz	4149.2	4149.5333(13)			4149.4
C_0 / MHz	3001.1	3000.69275(94)			3000.6
$v_{12} = 1$ (176 cm^{-1})					
A_0 / MHz	10,176.9	10,157.64443(76)			10,168.7
B_0 / MHz	4176.8	4175.90448(37)			4176.9
C_0 / MHz	3006.3	3005.52426(35)			3005.9

[1] Equilibrium rotational constants (B^{eq}) from CCSD(T)/CBS + CV equilibrium structure augmented by vibrational corrections (ΔB^{v}) at the MP2/aug-cc-pVTZ level. Best-estimated quartic centrifugal-distortion constants from the 'cheap' scheme. Sextic centrifugal-distortion constants at the MP2/aug-cc-pVTZ level. For details, see Ref 165.
[2] Ref 166.
[3] Scaled parameters obtained by employing Eq. (25).

intense IR bands related to the C-H stretching vibrations of *gauche*-EtSH and to the N-H stretchings of cytosine. For *gauche*-EtSH, with computations at the CCSD(T)/cc-pVTZ level, the so-called 'SkipPT2' approach leads to MAE and |MAX| of 4.5 and 7 cm^{-1}, respectively. A slightly lower accuracy is observed for cytosine (MAE = 15 cm^{-1} and |MAX| =21 cm^{-1}), as expected from QM computations at the B3LYP level.[144] As noted before, the accuracy can indeed be improved with GVPT2 computations based on CC/DFT hybrid force fields. However, it might be unclear *a priori* whether the LAMs contaminate the GVPT2 treatment of high-frequency vibrations or not. To address this point, we can consider the case of methyloxirane that shows a barrier for the internal rotation of the methyl group of 893 cm^{-1}.[153] It has been shown that in this case, the full GVPT2 treatment using the 'cheap'/B3LYP hybrid force field leads to highly accurate wavenumbers, with a mean absolute deviation of 4.8 cm^{-1} and a maximum error below 18 cm^{-1} for all fundamental vibrations, even for the C-H stretchings and the torsion of the methyl group.[31] Interestingly, the reduced model with the methyl torsion excluded from VPT2 shows results very similar to the full GVPT2 approach for all C-H stretching vibrations, but with improved mean and maximum errors with respect to experiment, reduced to 4 and 8 cm^{-1}, respectively. This indicates that the reduced-dimensionality, LAM-free GVPT2 models represent a reliable approach for accurate vibrational computations and should be preferred in

presence of LAMs, especially if the actual impact of the latter on the rest of the system cannot be assessed univocally.

Conformers

As mentioned above, the rotational spectrum of molecular species that exhibit LAMs can be a challenge for both computational and experimental molecular spectroscopies. AstroCOMs of increasing size and complexity are often characterized by high flexibility due to rotations around single bonds. On general grounds, the presence of LAMs implies molecular flexibility, which in turn leads to the existence of several conformers. The analysis of the rotational and vibrational spectra might therefore be hampered by the concomitant presence of different conformers, thus requiring the accurate determination of their relative energies. The situation can be further complicated by the fact that the relative energies of the lowest-excited vibrational states of the most stable conformer might be similar to those of the vibrational ground states of less stable species.

A noteworthy example is the rotational spectrum of glycine (NH_2CH_2COOH), the smallest amino acid, which has been found in several carbonaceous meteorites, and is one of the two most abundant amino acids in Stardust-returned foil samples,[27] but its presence in the ISM has not yet been confirmed. As pointed out in Refs 16, regarding its search in hot-core sources (i.e., in environment at T ~200 K) the second most stable conformer, IIn, is more important than the first one, glycine Ip. In fact, at a temperature of about 200 K, despite the relative population of the conformer IIn being only ~10%, its rotational spectrum is more intense than that of the most abundant Ip conformer. This is due to the larger dipole moment components of glycine IIn with respect to those of glycine Ip (see Figure 1). However, the correct evaluation of their relative energy is of fundamental importance. Figure 5 shows how the relative intensity of the rotational spectrum changes depending on the energy difference between Ip and IIn. The CDMS database reports a value of about 700 cm^{-1},[179] which implies at T = 200 K a population for the IIn conformer lower than 1% (using the relative energy instead of the free energy to estimate the population ratio). The consequence is that, as seen in the left side of Figure 5, the rotational spectra of the two conformers have approximately the same intensity. On the other hand, if a value of 312 cm^{-1}, obtained at the CCSD(T)/CBS + CV level (also including ZPVE correction),[29] is considered, the rotational spectrum of the IIn conformer results to be about four times more intense than that of glycine Ip (see right side of Figure 5). While the accurate evaluation of the relative energy of glycine conformers is addressed in the following, we point out that the results presented here, and the significant population of glycine IIn already at 200 K, have an important impact on the attempt of identifying glycine in space. Indeed, on the basis of the recent literature glycine could reach detectable levels in cold solar-type system precursors[180] or hot-core sources.[181] The rotational spectrum of the most stable conformer of glycine is expected to have peak intensities greater than 10 mK in the ALMA band 2 (68–90 GHz) for detections from a solar-type system precursor, like the L1544 pre-stellar core.[180] For pre-stellar core systems, due to their characteristic, very low temperatures, it is fully justified to consider that only the most stable conformer, Ip, is present. However, only glycine Ip has also been considered for the simulation of the emission spectra of the hot-core source NGC 6334 IRS1,[181] with a characteristic temperature of 200 K.

More exhaustively, with respect to the notation used above, the glycine conformers are denoted

TABLE 6 | Theoretical Predictions of the Large-Amplitude Fundamentals (ω and ν in cm^{-1}), as Obtained from the Two-Dimensional (2D) Variational and GVPT2 Treatments, Compared to Experiment

	Harmonic[1]	2D variational[2]	GVPT2[1]	Experiment[3]	
astroCOMs	ω	ν	ν	ν	Assignment
gauche-EtSH	201	189.61	191	193.0	(–)SH torsion
		188.13		191.8	(+)SH torsion
	259	254.07	251	247.5	(–)CH torsion
		254.05			(+)CH torsion
trans-EtSH	179	155.74	171	158.0	SH torsion
	255	245.20	248		CH torsion

[1] Computations at the CCSD/cc-pVTZ level, see Ref 178.
[2] Computations at the CCSD(T)/aug-cc-pVTZ level, see Ref 178 .
[3] Experimental wavenumbers as reported in Ref 178.

TABLE 7 | Theoretical Predictions of High-Frequency Vibrations (ω and ν in cm^{-1}) Coupled with Large Amplitude Motion, Compared to Experiment

	Harmonic	GVPT2 Full	GVPT2 Skip[1]	Experiment[2]	
astroCOMs	ω	ν	ν	ν	Assignment
gauche-EtSH[3]	3110	3033	2969	2967	CH stretch
	3130	2958	2987	2980	CH_2 stretch
cytosine[4]	3597	3473	3438	3441	NH_2 sym stretch
	3617	3452	3450	3472	N_1H stretch
	3733	3604	3540	3564	NH_2 asym stretch
methyloxirane[5]	3039	2961	2959	2942	CH_3 sym stretch
	3110	3015	3015		CH_2 sym stretch
	3117	2978	2973	2974	CH_3 asym stretch
	3120	2993	2991	2995	CH_3 asym stretch
	3139	3001	2998	3001	CH stretch
	3204	3058	3058	3051	CH_2 asym stretch
MAE[6]	142	21	9		
|MAX|[6]	169	66	24		

[1] Low-frequency large-amplitude modes excluded from the GVPT2 treatment.
[2] Experimental wavenumbers as compiled in: Ref 178 for *gauche*-ethyl mercaptan, Ref 144 for cytosine, and Ref 31 for methyloxirane.
[3] Computations at the CCSD(T)/cc-pVTZ level, see Ref 178.
[4] Computations at the B3LYP/SNSD level, see Ref 144.
[5] Computations at the 'cheap'/B3LYP level see Refs 31,65.
[6] Mean absolute error (MAE) and maximum absolute deviations (|MAX|) (in cm^{-1}) with respect to the experimental wavenumbers.

using, in addition to the number for the stability order and the 'p,n' labels for the planarity or nonplanarity of the backbone, respectively, the 'c,t' labels for indicating the *cis* or *trans* orientation with respect to the three torsional angles. According to this notation,[182] the three conformers observed in the gas phase are Ip/ttt, IIn/ccc, and IIIp/tct (the recently observed short-lived highly energetic VIp/ttc[183,184] is not relevant in the astrochemical context; see Refs 29 for extended discussion). Among the torsional degrees of freedom, those around the C–N and C–C bonds are also LAMs. In addition to the problem of getting correct spectroscopic properties as described above, they represent also a challenging aspect for the accurate calculation of thermochemical properties.[60,185–188] In this case as well, a feasible route is to partition the molecular Hamiltonian between large- and small-amplitude motions, which can be treated at different levels of accuracy.[188] In this respect, within the hindered-rotor anharmonic-oscillator (HRAO) model, the modes identified as large-amplitude, hindered-rotor motions[185] are treated separately and considered inactive in the vibrational perturbative computations. The HRAO approach, in conjunction with HDCPT2 computations and simple perturbation theory (SPT),[189] represents a viable route for reliable computations of thermodynamic properties.[60]

Table 8 collects the theoretical prediction of the gas-phase thermodynamic properties of the glycine conformers at 15, 200, and 410 K. These three temperatures have been selected as they correspond to different types of astrochemical environments: from the cold interstellar regions to the hot cores, and finally toward the temperature limits for the detection of glycine before its decomposition at 506 K. All predictions are based on the best estimates of relative electronic energies at the CCSD(T)/CBS + CV level in conjunction with thermodynamic properties derived from either the standard RRHO model or the more accurate HRAO scheme, with the anharmonic PES computed at the 'cheap'/B3LYP level.[29] Boltzmann populations of the Ip/ttt and IIn/ccc conformers at different temperatures, derived from the data collected in CDMS,[179] are also reported for comparison purposes. All data agree that only the most stable conformer can be present at 15 K, despite differences in the prediction of relative energies up to 5 kJ mol^{-1}. The situation is much different at higher temperatures. In particular, we can note that the RRHO model strongly overestimates the population of the IIIp/tct rotamer, which is predicted to have a population of about 10% at 200 K and over 50% at 410 K, thus meaning a population larger than that of the Ip/ttt confomer. At variance, the full HRAO approach is able to provide a reasonable relative free energy for this conformer at all temperatures, in good agreement with experimental laboratory observations.[190] The differences between the results obtained

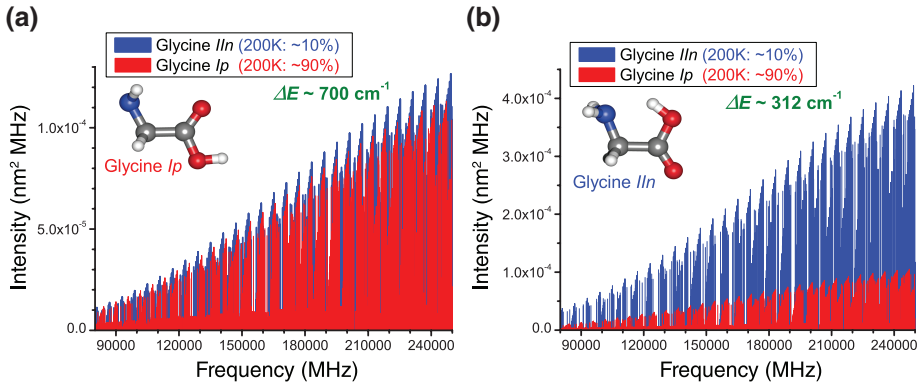

FIGURE 5 | Simulation of the rotational spectra of glycine Ip and IIn at T = 200 K in the 80–250 GHz frequency range. Spectroscopic parameters are taken from the Cologne Database for Molecular Spectroscopy (CDMS) database,[179] while the population ratio is based on an energy difference of either 700 cm^{-1} (left, Ref 179) or 312 cm^{-1} (right, Ref 29).

with RRHO and HRAO are significant also for the IIn/ccc conformer, for which our best theoretical estimates predict non-negligible abundances of about 10% at 200 K and 20% at 410 K.

As addressed for the detection of rotational features, also in the case of IR observations, it is necessary to identify the most stable conformers and to assess the probability of their detection in the astronomical environments, which might vary considerably depending on space-like conditions and spectral ranges. Considering the detection of glycine by means of its signatures in the MIR region, and according to the discussion above, we should conclude that the Ip/ttt conformer gives the strongest signals due to its largest population at all temperatures and to the fact that the most characteristic bands show similar intensity. Of interest to the present discussion is that extremely accurate results have been obtained by applying the GVPT2 approach to the 'cheap'/B3LYP hybrid force field, thus providing accurate predictions for the most intense C = O stretching vibration (the so-called Amide I), i.e., with an accuracy of ± 5 cm^{-1} for all glycine conformers.[29] This finding is of relevance to the detection of glycine, and other prebiotic molecules, in complex astrophysical environments, thus allowing the distinction of the different conformers in the fingerprint spectral range.[16]

CHALLENGES IN COMPUTATIONAL CHEMISTRY OF ASTROCOMS

The evidence that a fairly rich chemistry is taking place across the Universe and the discovery of biomolecular precursors in the interstellar space raise the issue of the origins of terrestrial life, whose elucidation is one of the goals of Astrochemistry. Two alternative theories have been suggested so far[1]: exogenous and[2] endogenous synthesis. In the first theory, prebiotic molecules came from space, the carriers being comets, asteroids, and meteorites.[191] The rationale behind this suggestion is that plenty of astroCOMs have been observed in interstellar clouds. In the frame of this theory, it is of fundamental importance not only to discover prebiotic species in space, but also to understand how they could be produced in the typically harsh conditions (extremely low temperature and density) of the ISM. In the endogenous theory, the synthesis of simple organic molecules having a potential relation to the origin of life occurred directly on our planet starting from simple parent molecules in the atmosphere, liquid water, and various energy sources. The Urey-Miller experiment was a milestone in this theory.[192,193] In this context, Titan has been postulated to represent a model of primitive Earth.[194] Therefore, the organic chemistry in Titan's atmosphere could be directly linked to prebiotic organic synthesis in the atmosphere of our primitive planet.

Formation Routes

As briefly addressed above, one of the challenges of Astrochemistry is to understand how the molecular complexity gradually evolves from simple atomic or diatomic species to astroCOMs, and toward biological macromolecules, the building blocks of life. Focusing on astroCOMs, a good understanding of the possible formation/destruction pathways and of the associated thermochemistry and kinetics is necessary to fully exploit the currently available and future observational data as well as to prepare new

TABLE 8 | Theoretical[1] Thermodynamic Properties (kJ mol^{-1}) of the Three Experimentally Observed Glycine Conformers

	CDMS[2]				ΔE + ZPVE[3]						ΔG					
	Ip/ttt		IIn/ccc		Ip/ttt		IIn/ccc		IIIp/tct		Ip/ttt		IIn/ccc		IIIp/tct	
	kJ mol^{-1}	%	kJ mol^{-1}	%	kJ mol^{-1}	%	kJ mol^{-1}	%	kJ mol^{-1}	%	kJ mol^{-1}	%	kJ mol^{-1}	%	kJ mol^{-1}	%
15 K																
RRHO	0	100	8.37	<0.01	0	100	3.82	<0.01	7.48	<0.01	0	100	3.82	<0.01	7.34	<0.01
HRAO[4,5]					0	100	3.73	<0.01	7.94	<0.01	0	100	3.72	<0.01	7.87	<0.01
200 K																
RRHO		99.4		0.6		90.0		9.0		1.0	0	82.5	4.24	6.4	3.34	11.1
HRAO[4,5]						89.7		9.5		0.8	0	88.7	3.53	10.6	8.08	0.7
410 K																
RRHO		92.1		7.9		66.9		22.7		7.7	0	38.3	5.41	7.9	−1.17	53.9
HRAO[4,5]						66.8		23.4		6.8	0	75.1	4.41	20.6	9.72	4.3

[1] Conformational energies with respect to the Ip/ttt conformer. All thermodynamic properties have been computed at 1 atm.
[2] Ref 179.
[3] CCSD(T)/CBS + CV energy computed at the corresponding optimized geometry and corrected for ZPVE at the 'cheap'/B3LYP level.
[4] The two lowest vibrations have been described by hindered-rotor contributions computed by means of an automatic procedure.[185]
[5] Contributions computed by means of the HDCPT2[60] model using the hybrid 'cheap'/B3LYP force field in conjunction with simple perturbation theory (SPT)[60,189] (see text for details).

observations. Since laboratory experiments are often not able to reproduce adequately the extreme conditions that characterize the ISM, accurate state-of-the-art computational approaches play a fundamental role to derive possible reaction mechanisms. Therefore, quantum-chemical calculations are increasingly exploited. Indeed, quantum chemistry has demonstrated to be a powerful tool to obtain reliable input parameters for astrochemical models, which in turn lead to simulated abundances (see for instance Refs 195 and 196 for further details). Therefore, reaction schemes with all relevant pathways need to be formulated, thus requiring the identification of all intermediate species, from reactants to products, as well as of the transition states connecting them. In practical terms, accurate electronic structure calculations should be carried out for every chemical species involved in the reaction scheme in order to obtain structure, energies, spectroscopic properties, and from them thermochemical quantities. From those data, kinetic rate constants can in turn be computed. While a detailed discussion on the theoretical background of reaction kinetics would be far beyond the scope of this review, it is worthwhile noting that a variety of models are available to estimate rate constants, with very diverse levels of complexity.[197] In this review, we have limited ourselves to the transition state theory.[198,199] An appealing aspect of this theory is that it only requires the definition of the reactants and/or products and the transition state and the required data, which depend on the chosen model, at those geometries. Further details can be found in Refs 198–200 and in the articles cited in the examples below.

From a practical point of view on the subject of interest here, a survey of the available literature reveals that much information is still lacking and only a small fraction of the elementary reactions has been characterized. The mechanisms leading to astro-COMs in star forming regions are still object of debate, although it is clear that the synthesis can proceed via chemical reactions on the surface of (icy) dust grains or in the gas phase.[201] Both synthetic routes represent great challenges for quantum chemistry, with the key point being the very accurate evaluation of the energetics: the reaction to occur in the harsh conditions typical of the ISM requires that all transition states lie below the reactant asymptotes, since there is no additional source of energy to overcome energy barriers. The vicinity of the energy levels of the transition states and the reactant asymptotes is a real computational challenge because the status of the transition states as 'emerged' or 'submerged' can fall within the uncertainty of the calculations. In this

respect, the recent investigation of the gas-phase formation route of formamide provides a significant example.[33] Formamide ($HCONH_2$) has a peculiar role in prebiotic chemistry because it can generate both genetic and metabolic molecules (see for instance Refs 202). According to Refs 33, the NH_2 + H_2CO reaction proceeds with the formation of a bound intermediate. Along the reaction path, a van der Waals complex is formed and a transition state has to be surmounted to reach the addition intermediate (see Figure 6). Then, a second transition state connects the bound intermediate to the final products. It should be noted that, for this particular case, the relative energy of the transition state is above the reactant asymptotes. However, the issue here is whether this transition state is significantly above the reactants or not. The results at different levels of theory are collected in Figure 6. It is noteworthy that at the CCSD(T)/CBS + CV level, the energy of the transition state is slightly above the energy of the reactants' asymptote. However, when a fT and fQ excitations are also included, thus leading to the CCSD(T)/CBS + CV + fT and CCSD(T)/CBS + CV + fT + fQ approaches, the barrier related to this transition state decreases significantly, dropping from 3.77 to 2.05 kJ mol^{-1} with full-T and to 1.67 kJ mol^{-1} with full-T and full-Q. From Figure 6, the inadequacy of the CCSD(T)/maug-cc-pVTZ level of theory is evident, while the good performance of the B2PLYP functional in conjunction with the D3 dispersion correction,[203] even if clearly due to a compensation of errors, is encouraging for the investigation of larger systems.

Chemical Evolution

Recent measurements have revealed that Titan's atmosphere contains significant quantities of carbon (~2% CH_4) and nitrogen (98% N_2), and traces of oxygen (~50 ppm CO).[194] Therefore, the photochemical production of complex molecules containing C, N, O, and H is possible. Due to its reducing atmosphere and its rich and complex organic chemistry (see Refs 204 and references therein), Titan is thought to represent a model of primitive Earth. The investigation of Titan's atmosphere might therefore provide a unique opportunity to shed light on the organic evolution undertaken in the atmosphere of early Earth. Furthermore, Cassini measurements have revealed the presence of numerous large carbocations and carbanions in Titan's upper atmosphere (see Refs 204 and references therein). No other planets or satellites in our solar system have been found to bear the same level of chemical complexity as observed on Titan. There is an increasing complexity moving from the upper atmosphere to the ground: prebiotic molecules in Titan's upper atmosphere evolve to lead to the formation of macromolecules, the subsequent step is the assembly in a haze layer followed by the precipitation and sedimentation of complex organics on the surface, where the final organic catalysis in the hydrocarbon lakes occurs.

In Refs 204, reaction mechanisms have been proposed to describe the growth process of the complex macromolecules observed by the mass spectrometers onboard Cassini. Figure 7 shows the initial steps of the formation of macromolecules, focusing on plausible reaction routes from simple aromatic molecules to complex polyaromatic compounds. Once confirmed, the proposed reaction mechanisms will provide the first step toward understanding how aromatic molecules and macromolecules (also including the formation of heterocycles) were produced in the atmosphere of primitive Earth. In particular, in Refs 204, the phenalenyl cation $C_{13}H_9^+$ and its anion $C_{13}H_9^-$ were identified as important intermediates in the process of molecular growth. An important confirmation of the plausibility of the proposed mechanisms would be the astronomical observation of the spectroscopic features of $C_{13}H_9^+$ and $C_{13}H_9^-$, for which however there is a great paucity of spectroscopic information. Being highly symmetric, these molecular species lack a permanent electric dipole moment and their detection relies only on IR spectroscopy. In this respect, the great opportunity offered by JWST should be pointed out. In Figure 8, the fully anharmonic IR spectra of the phenalenyl cation and anion, computed at the B3LYP/6–31 + G (d,p) level, are shown. For this level of theory, from the literature on this topic based on the comparison with experiment and state-of-the-art calculations (see Refs 62,133,205), a mean absolute error of 10–12 cm^{-1} and maximum discrepancies of 30 cm^{-1} are expected, which provide a reasonable guidance for astronomical detections, with possible improvements through hybrid schemes as discussed above. However, the phenalenyl cation and anion represent a complex case for VPT2 calculations. First, as symmetric tops, a proper account of degeneracies, ignored in the present discussions, is necessary. Second, the out-of-plane ring deformation mode acts as a LAM, thus contaminating the anharmonic results, and must be adequately decoupled from the rest of the system, in a way similar to the 'SkipPT2' scheme discussed before. Finally, being large-sized molecules, they also bear a significant number of resonances, in

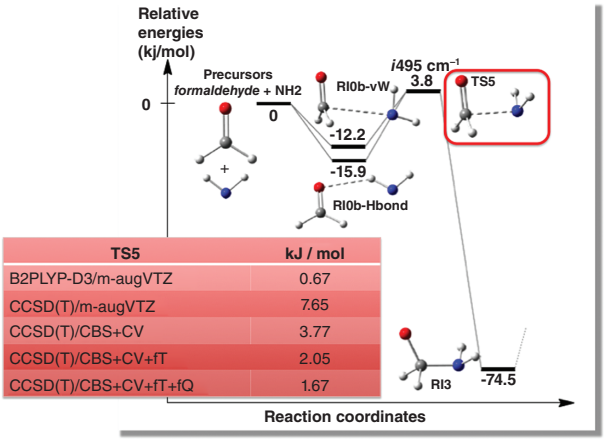

FIGURE 6 | First steps of the NH_2 + formaldehyde (H_2CO) reaction mechanism. Relative electronic CCSD(T)/CBS + CV energies (in kJ mol^{-1}) in black. Minima and transition states are labeled according to the notation of Ref 33 In the inset: the relative energy of the TS5 transition state at different levels of theory is given (for details,see text).

particular the Darling–Dennison ones, which are rather sensitive to the quality of the electronic structure calculation and also need to be properly assessed and corrected.

CONCLUDING REMARKS

Some of the most challenging aspects in the field of computational chemistry applied to Astrochemistry have been reviewed. The molecular complexity in space was first addressed to explain the importance of the support of computational spectroscopy to astrochemical investigations. To fully exploit the possibilities offered by computational spectroscopy in the study of gaseous species, from the micro- to the IR wavelengths, a comprehensive summary of the underlying rovibrational theory was first given, followed by a description of state-of-the-art protocols for the simulation of small-to-medium sized astroCOMs with the required accuracy. The methodology and its different technical aspects were then illustrated through a test case, oxirane—an example of semirigid astroCOM, demonstrating the accuracy of theoretical predictions for rotational and vibrational spectroscopic features. Subsequently, the challenges in the computational spectroscopy of astroCOMs have been faced: by means of selected examples, the most relevant aspects have been introduced, discussed, and properly addressed. Finally, we moved to deal with the challenges in the computational chemistry of astroCOMs. While spectroscopy offers the opportunity to study, discover, and quantify

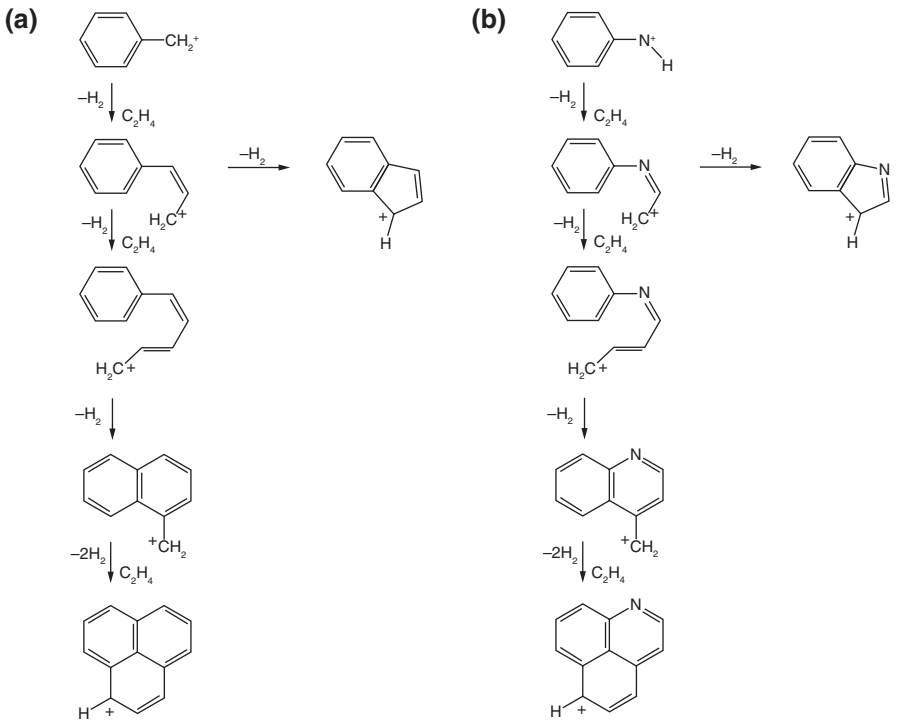

FIGURE 7 | Reaction pathways of the progression of chain reactions of C_2H_4 with (a) $C_7H_7^+$ and (b) $C_6H_5NH^+$ to elucidate the formation mechanism of (N-)heterocycles.

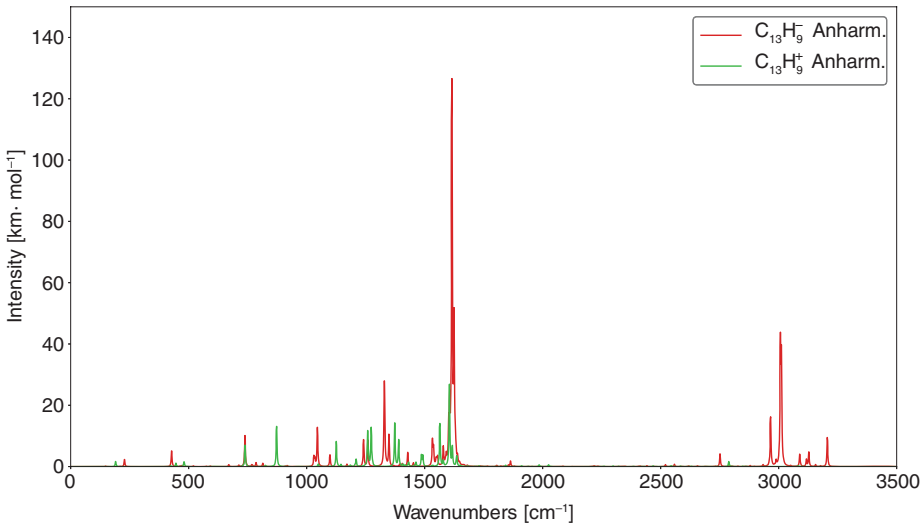

FIGURE 8 | Simulated infrared (IR) spectra of $C_{13}H_9^+$ and $C_{13}H_9^-$. Anharmonic wavenumbers and intensities were computed at the B3LYP/ 6–31 + G(d,p) level of theory and the stick spectra convoluted by means of Lorentzian broadening functions with half-widths at half maximum of 2 cm^{-1}.

molecular species in space, computational chemistry allows understanding how astroCOMs could be produced in the typically harsh conditions of the ISM. The challenges in evaluating feasible formation routes of relevant prebiotic species as well as in understanding the chemical evolution of small species toward macromolecules have been addressed. To summarize, we demonstrated that, even for cases that are challenging for both experiment and theory, the use of the proper combination of state-of-the-art QM approaches and effective treatments of nuclear problems leads to the quantitative prediction of the spectroscopic and thermochemical properties. The chosen examples and their discussion have shown that rotational constants, which are the leading terms in rotational spectroscopy, can be predicted with an accuracy, in relative terms, better than 0.1% and that this accuracy can be further improved (by about one order of magnitude) by means of an empirical scaling procedure. Moving to vibrational signatures, the typical MAE and |MAX| for fundamentals are better than 10 and 15 cm^{-1}, respectively. Concerning energetics, the importance of accurately determining energy differences of conformers has been pointed out, with the state-of-the-art computational approaches presented here able to provide gas-phase thermodynamic properties with an accuracy better than 1 kJ mol^{-1}.

In the last years, a close collaboration between astronomers and spectroscopic laboratories has allowed the identification of thousands of unknown lines (due, in most cases, to 'weeds'). However, in addition to neutral, closed-shell molecules, ionic and radical species are also present in space. They provide an additional challenge in Astrochemistry. Their experimental investigation is strongly hampered by the difficulties in their on-the-fly production and their instability, and thus is not always feasible. On the other hand, state-of-the-art QM approaches are able to compute spectroscopic parameters with the same accuracy as demonstrated for closed-shell molecules. Computational spectroscopic characterizations can therefore be used to guide laboratory experiments, and when the latter are not viable, calculations (possibly further improved by the empirical scaling procedure) can be directly used to support astronomical searches. However, from a theoretical point of view, new developments are required in order to improve the predictive capabilities because of the lack of implementations. To give an example, to the best of our knowledge, a CCSD(T) implementation for the computation of electron spin-nuclear spin coupling constants, important for the prediction of the rotational spectrum of radicals, is still missing.

ACKNOWLEDGMENTS

This work has been supported in Bologna by MIUR 'PRIN 2015' funds (project 'STARS in the CAOS (Simulation Tools for Astrochemical Reactivity and Spectroscopy in the Cyberinfrastructure for

Astrochemical Organic Species)'—Grant Number 2015F59J3R) and by the University of Bologna (RFO funds), and in Shanghai by National Natural Science Foundation of China (Grant No. 91641128). The SMART@SNS Laboratory (http://smart.sns.it) is gratefully acknowledged for the utilization of computer resources. The support of the COST CMTS-Actions CM1405 (MOLIM: MOLecules in Motion) and CM1401 (Our Astro-Chemical History) is acknowledged. The authors also acknowledge Dr. Lorenzo Spada for fruitful discussions.

FURTHER READING

ASTROCHEMISTRY

1. Yamamoto S. *Introduction to Astrochemistry Chemical Evolution from Interstellar Clouds to Star and Planet Formation*. Berlin, Heidelberg: Springer; 2017.
2. Williams DA, Viti S. *Observational Molecular Astronomy Exploring the Universe Using Molecular Line Emissions*. Cambridge: Cambridge University Press; 2013.
3. Kwok S. *Organic Matter in the Universe*. Weinheim: Wiley; 2012.
4. Schlemmer S, Giesen T, Mutschke H, eds. *Laboratory Astrochemistry: From Molecules through Nanoparticles to Grains*. Weinheim: Wiley; 2011.
5. Tennyson J. *A Stronomical Spectroscopy. An Introduction to the Atomic and Molecular Physics of Astronomical Spectra*. 2nd ed. World Scientific; 2011.
6. "The Astrochymist" website. Available at: http://www.astrochymist.org/

QUANTUM MECHANICS

1. Helgaker T, Jørgensen P, Olsen J. *Electronic-Structure Theory*. Wiley; 2000.
2. Szabo A, Ostlund NS. *Modern Quantum Chemistry*. MacMillan Publishing Co., Inc.; 1982.
3. Shavitt I, Bartlett RJ. *Many-Body Methods in Chemistry and Physics*. Cambridge University Press; 2009.

SPECTROSCOPY

1. Quack M, Merkt F. *Handbook of High-Resolution Spectroscopy*. Wiley; 2011.
2. Barone V, ed. *Computational Strategies for Spectroscopy, from Small Molecules to Nano Systems*. Princeton, NJ: John Wiley & Sons; 2011.
3. Califano S. *Vibrational States*. Hoboken, NJ: John Wiley & Sons; 1976.
4. Herzberg G. *Molecular Spectra and Molecular Structure: I. Spectra of Diatomic Molecules*. D. Princeton, NJ: Van Nostrand Company; 1950.
5. Wilson EB Jr, Decius JC, Cross PC. *Molecular Vibrations*. New York City, NY: McGraw-Hill Book Company, Inc.; 1955.

REFERENCES

1. Müller HSP, Schlöder F, Stutzki J, Winnewisser G. The Cologne Database for Molecular Spectroscopy, CDMS: a useful tool for astronomers and spectroscopists. *J Mol Struct* 2005, 742:215–227. https://doi.org/10.1016/j.molstruc.2005.01.027.
2. Endres CP, Schlemmer S, Schilke P, Stutzki J, Müller HS. The Cologne Database for Molecular Spectroscopy, CDMS, in the Virtual Atomic and Molecular Data Centre, VAMDC. *J Mol Spectrosc* 2016, 327:95–104. https://doi.org/10.1016/j.jms.2016.03.005.

3. Herbst E, Yates JT. Introduction: Astrochemistry. *Chem Rev* 2013, 113:8707–8709. https://doi.org/10.1021/cr400579y.

4. Brown WA. Astrochemistry. *Phys Chem Chem Phys* 2014, 16:3343. https://doi.org/10.1039/C4CP90004A.

5. Schlemmer S, Mutschke H, Giesen T, Jäger C. *Laboratory Astrochemistry: From Molecules through Nanoparticles to Grains*. Berlin: Wiley-VCH Verlag GmbH & Co.; 2015.

6. Woon DE, Herbst E. Quantum chemical predictions of the properties of known and postulated neutral interstellar molecules. *Astrophys J Suppl Ser* 2009, 185:273–288. https://doi.org/10.1088/0067-0049/185/2/273.

7. Yu Q, Bowman JM, Fortenberry RC, Mancini JS, Lee TJ, Crawford TD, Klemperer W, Francisco JS. Structure, anharmonic vibrational frequencies, and intensities of $NNHNN^+$. *J Phys Chem A* 2015, 119:11623–11631. https://doi.org/10.1021/acs.jpca.5b09682.

8. Bauschlicher CW Jr, Peeters E, Allamandola LJ. The infrared spectra of very large irregular polycyclic aromatic hydrocarbons (PAHs): observational probes of astronomical PAH geometry, size, and charge. *Astrophys J* 2009, 697:311–327. https://doi.org/10.1088/0004-637X/697/1/311.

9. Peverati R, Bera PP, Lee TJ, Head-Gordon M. Insights into hydrocarbon chain and aromatic ring formation in the interstellar medium: computational study of the isomers of $C_4H_3^+$, $C_6H_3^+$ and $C_6H_5^+$ and their formation pathways. *Astrophys J* 2016, 830:128 https://doi.org/10.3847/0004-637X/830/2/128.

10. Finney B, Fortenberry RC, Francisco JS, Peterson KA. A spectroscopic case for SPSi detection: the third-row in a single molecule. *J Chem Phys* 2016, 145:124311 https://doi.org/10.1063/1.4963337.

11. Fortenberry RC. Quantum astrochemical spectroscopy. *Int J Quantum Chem* 2017, 117:81–91. https://doi.org/10.1002/qua.25180.

12. Puzzarini C. Astronomical complex organic molecules: quantum chemistry meets rotational spectroscopy. *Int J Quantum Chem* 2017, 117:129–138. https://doi.org/10.1002/qua.25284.

13. Candian A, Mackie CJ. Anharmonic interstellar PAH molecules. *Int J Quantum Chem* 2017, 117:146–150. https://doi.org/10.1002/qua.25292.

14. Tennyson J, Yurchenko SN. The ExoMol project: software for computing large molecular line lists. *Int J Quantum Chem* 2017, 117:92–103. https://doi.org/10.1002/qua.25190.

15. Tennyson J. Accurate variational calculations for line lists to model the vibration-rotation spectra of hot astrophysical atmospheres. *Wiley Interdiscip Rev Comput Mol Sci* 2011, 2:698–715. https://doi.org/10.1002/wcms.94.

16. Barone V, Biczysko M, Puzzarini C. Quantum chemistry meets spectroscopy for Astrochemistry: increasing complexity toward prebiotic molecules. *Acc Chem Res* 2015, 48:1413–1422. https://doi.org/10.1021/ar5003285.

17. Primos. Available at: http://www.cv.nrao.edu/~aremijan/PRIMOS/. (Accessed May 5, 2017)

18. Neill JL, Muckle MT, Zaleski DP, Steber AL, Pate BH, Lattanzi V, Spezzano S, McCarthy MC, Remijan AJ. Laboratory and tentative interstellar detection of trans-methyl FORMATE using the publicly available Green Bank Telescope PRIMOS survey. *Astrophys J* 2012, 755:153 https://doi.org/10.1088/0004-637X/755/2/153.

19. McGuire BA, Carroll PB, Loomis RA, Finneran IA, Jewell PR, Remijan AJ, Blake GA. Discovery of the interstellar chiral molecule propylene oxide (CH_3CHCH_2O). *Science* 2016, 352:1449–1452. https://doi.org/10.1126/science.aae0328.

20. Puzzarini C, Biczysko M, Bloino J, Barone V. Accurate spectroscopic characterization of oxirane: a valuable route to its identification in TITAN'S atmosphere and the assignment of unidentified infrared bands. *Astrophys J* 2014, 785:107. https://doi.org/10.1088/0004-637X/785/2/107.

21. Rubin RH, Swenson GW Jr, Benson RC, Tigelaar HL, Flygare WH. Microwave detection of interstellar formamide. *Astrophys J* 1971, 169:L39 https://doi.org/10.1086/180810.

22. Dickens JE, Irvine WM, Ohishi M, Ikeda M, Ishikawa S, Nummelin A, Hjalmarson Å. Detection of interstellar ethylene oxide (c-C_2H_4O). *Astrophys J* 1997, 489:753–757. https://doi.org/10.1086/304821.

23. Hollis JM, Jewell PR, Lovas FJ, Remijan A, Møllendal H. Green Bank telescope detection of new interstellar aldehydes: propenal and propanal. *Astrophys J Lett* 2004, 610:L21–L24. https://doi.org/10.1086/423200.

24. Kolesniková L, Tercero B, Cernicharo J, Alonso JL, Daly AM, Gordon BP, Shipman ST. Spectroscopic characterization and detection of ethyl Mercaptan in Orion. *Astrophys J Lett* 2014, 784:L7 https://doi.org/10.1088/2041-8205/784/1/L7.

25. Kuan Y-J, Charnley SB, Huang H-C, Tseng W-L, Kisiel Z. Interstellar glycine. *Astrophys J* 2003, 593:848–867. https://doi.org/10.1086/375637.

26. Snyder LE, Lovas FJ, Hollis JM, Friedel DN, Jewell PR, Remijan A, Ilyushin VV, Alekseev EA, Dyubko SF. A rigorous attempt to verify interstellar glycine. *Astrophys J* 2005, 619:914–930. https://doi.org/10.1086/426677.

27. Elsila JE, Glavin DP, Dworkin JP. Cometary glycine detected in samples returned by stardust. *Meteorit Planet Sci* 2009, 44:1323–1330. https://doi.org/10.1111/j.1945-5100.2009.tb01224.x.

28. Callahan MP, Smith KE, Cleaves HJ, Ruzicka J, Stern JC, Glavin DP, House CH, Dworkin JP. Carbonaceous meteorites contain a wide range of extraterrestrial nucleobases. *Proc Nat Acad Sci USA* 2011, 108:13995–13998. https://doi.org/10.1073/pnas.1106493108.

29. Barone V, Biczysko M, Bloino J, Puzzarini C. Accurate structure, thermodynamic and spectroscopic parameters from CC and CC/DFT schemes: the challenge of the conformational equilibrium in glycine. *Phys Chem Chem Phys* 2013, 15:10094–10111. https://doi.org/10.1039/C3CP50439E.

30. Barone V, Biczysko M, Bloino J, Cimino P, Penocchio E, Puzzarini C. CC/DFT route toward accurate structures and spectroscopic features for observed and elusive conformers of flexible molecules: pyruvic acid as a case study. *J Chem Theory Comput* 2015, 11:4342–4363. https://doi.org/10.1021/acs.jctc.5b00580.

31. Barone V, Biczysko M, Bloino J, Puzzarini C. Accurate molecular structures and infrared spectra of trans-2,3-dideuterooxirane, methyloxirane, and trans-2,3-dimethyloxirane. *J Chem Phys* 2014, 141:034107. https://doi.org/10.1063/1.4887357.

32. Puzzarini C, Biczysko M, Barone V, Largo L, Peña I, Cabezas C, Alonso JL. Accurate characterization of the peptide linkage in the gas phase: a joint quantum-chemical and rotational spectroscopy study of the glycine dipeptide analogue. *J Phys Chem Lett* 2014, 5:534–540. https://doi.org/10.1021/jz402744a.

33. Vazart F, Calderini D, Puzzarini C, Skouteris D, Barone V. State-of-the-art thermochemical and kinetic computations for astrochemical complex organic molecules: formamide formation in cold interstellar clouds as a case study. *J Chem Theory Comput* 2016, 12:5385–5397. https://doi.org/10.1021/acs.jctc.6b00379.

34. Tielens AGGM. The molecular universe. *Rev Mod Phys* 2013, 85:1021–1081. https://doi.org/10.1103/RevModPhys.85.1021.

35. Pesonen J, Halonen L. Recent advances in the theory of vibration-rotation Hamiltonians. In: Prigogine I, Rice SA, eds. *Advances in Chemical Physics*, vol 125. Hoboken: John Wiley & Sons, Inc.; 2003, 269–349. http://dx.doi.org/10.1002/0471428027.ch4.

36. Császár AG, Fábri C, Szidarovszky T, Mátyus E, Furtenbacher T, Czakó G. The fourth age of quantum chemistry: molecules in motion. *Phys Chem Chem Phys* 2012, 14:1085–1106. https://doi.org/10.1039/C1CP21830A.

37. Mátyus E, Czakó G, Császár AG. Toward black-box-type full- and reduced-dimensional variational (ro) vibrational computations. *J Chem Phys* 2009, 130:134112 https://doi.org/10.1063/1.3076742.

38. Carrington T Jr. Perspective: computing (ro-)vibrational spectra of molecules with more than four atoms. *J Chem Phys* 2017, 146:120902 https://doi.org/10.1063/1.4979117.

39. Szalay V. Eckart ro-vibrational Hamiltonians via the gateway Hamilton operator: theory and practice. *J Chem Phys* 2017, 146:124107 https://doi.org/10.1063/1.4978686.

40. Barone V. The virtual multifrequency spectrometer: a new paradigm for spectroscopy. *Wiley Interdiscip Rev Comput Mol Sci* 2016, 6:86–110. https://doi.org/10.1002/wcms.1238.

41. Carter S, Sharma AR, Bowman JM, Rosmus P, Tarroni R. Calculations of rovibrational energies and dipole transition intensities for polyatomic molecules using MULTIMODE. *J Chem Phys* 2009, 131:224106 https://doi.org/10.1063/1.3266577.

42. Rauhut G, Hrenar T. A combined variational and perturbational study on the vibrational spectrum of P_2F_4. *Chem Phys* 2008, 346:160–166. https://doi.org/10.1016/j.chemphys.2008.01.039.

43. Christiansen O. Selected new developments in vibrational structure theory: potential construction and vibrational wave function calculations. *Phys Chem Chem Phys* 2012, 14:6672–6687. https://doi.org/10.1039/C2CP40090A.

44. Roy TK, Gerber RB. Vibrational self-consistent field calculations for spectroscopy of biological molecules: new algorithmic developments and applications. *Phys Chem Chem Phys* 2013, 15:9468–9492. https://doi.org/10.1039/C3CP50739D.

45. Nielsen HH. The vibration-rotation energies of molecules. *Rev Mod Phys* 1951, 23:90–136. https://doi.org/10.1103/RevModPhys.23.90.

46. Amat G, Nielsen HH. Vibrational l-type doubling and l-type resonance in linear polyatomic molecules. *J Mol Spectrosc* 1958, 2:152–162. https://doi.org/10.1016/0022-2852(58)90070-5.

47. Mills IM. In: Rao KN, Mathews CW, eds. *Molecular Spectroscopy: Modern Research*. New York: Academic Press; 1972), chap. 3.2, 115–140. https://doi.org/10.1016/B978-0-12-580640-4.50013-3.

48. Mills IM. In: Dixon RN, ed. *Theoretical Chemistry: Volume 1*, vol. 1. Cambridge: The Royal Society of Chemistry; 1974, 110–159. https://doi.org/10.1039/9781847557124-00110.

49. Aliev MR, Watson JKG. In: Rao KN, ed. *Molecular Spectroscopy: Modern Research*, vol. 3. Cambridge, MA: Academic Press; 1985, 1–67. https://doi.org/10.1016/B978-0-12-580643-5.50006-3.

50. Clabo DA Jr, Allen WD, Remington RB, Yamaguchi Y, Schaefer HF III. A systematic study of molecular vibrational anharmonicity and vibration—rotation interaction by self-consistent-field higher-derivative methods. Asymmetric top molecules. *Chem Phys* 1988, 123:187–239. https://doi.org/10.1016/0301-0104(88)87271-9.

51. Allen WD, Yamaguchi Y, Császár AG, Clabo DA Jr, Remington RB, Schaefer HF III. A systematic study of molecular vibrational anharmonicity and vibration-rotation interaction by self-consistent-field higher-derivative methods. Linear polyatomic molecules. *Chem Phys* 1990, 145:427–466. https://doi.org/10.1016/0301-0104(90)87051-C.

52. Willets A, Handy NC, Green WH Jr, Jayatilaka D. Anharmonic corrections to vibrational transition intensities. *J Phys Chem* 1990, 94:5608–5616. https://doi.org/10.1021/j100377a038.

53. Amos RD, Handy NC, Green WH, Jayatilaka D, Willetts A, Palmieri P. Anharmonic vibrational properties of CH_2F_2: a comparison of theory and experiment. *J Chem Phys* 1991, 95:8323–8336. https://doi.org/10.1063/1.461259.

54. Gaw F, Willetts A, Handy N, Green W. SPECTRO - a program for derivation of spectroscopic constants from provided quartic force fields and cubic dipole fields. In: *Advances in Molecular Vibrations and Collision Dynamics*, vol. 1. Oxford: JAI Press; 1992, 169–185.

55. Vázquez J, Stanton JF. Simple(r) algebraic equation for transition moments of fundamental transitions in vibrational second-order perturbation theory. *Mol Phys* 2006, 104:377–388. https://doi.org/10.1080/00268970500290367.

56. Barone V. Anharmonic vibrational properties by a fully automated second-order perturbative approach. *J Chem Phys* 2005, 122:014108. https://doi.org/10.1063/1.1824881.

57. Krasnoshchekov SV, Isayeva EV, Stepanov NF. Numerical-analytic implementation of the higher-order canonical van Vleck perturbation theory for the interpretation of medium-sized molecule vibrational spectra. *J Phys Chem A* 2012, 116:3691–3709. https://doi.org/10.1021/jp211400w.

58. Rosnik AM, Polik WF. VPT2+K spectroscopic constants and matrix elements of the transformed vibrational Hamiltonian of a polyatomic molecule with resonances using Van Vleck Perturbation theory. *Mol Phys* 2014, 112:261–300. https://doi.org/10.1080/00268976.2013.808386.

59. Ringholm M, Jonsson D, Bast R, Gao B, Thorvaldsen AJ, Ekström U, Helgaker T, Ruud K. Analytic cubic and quartic force fields using density-functional theory. *J Chem Phys* 2014, 140:034103. https://doi.org/10.1063/1.4861003.

60. Bloino J, Biczysko M, Barone V. General perturbative approach for spectroscopy, thermodynamics, and kinetics: methodological background and benchmark studies. *J Chem Theory Comput* 2012, 8:1015–1036. https://doi.org/10.1021/ct200814m.

61. Bloino J, Barone V. A second-order perturbation theory route to vibrational averages and transition properties of molecules: general formulation and application to infrared and vibrational circular dichroism spectroscopies. *J Chem Phys* 2012, 136:124108 https://doi.org/10.1063/1.3695210.

62. Barone V, Biczysko M, Bloino J. Fully anharmonic IR and Raman spectra of medium-size molecular systems: accuracy and interpretation. *Phys Chem Chem Phys* 2014, 16:1759–1787. https://doi.org/10.1039/C3CP53413H.

63. Piccardo M, Bloino J, Barone V. Generalized vibrational perturbation theory for rotovibrational energies of linear, symmetric and asymmetric tops: theory, approximations, and automated approaches to deal with medium-to-large molecular systems. *Int J Quantum Chem* 2015, 115:948–982. https://doi.org/10.1002/qua.24931.

64. Bloino J. A VPT2 route to near-infrared spectroscopy: the role of mechanical and electrical anharmonicity. *J Phys Chem A* 2015, 119:5269–5287. https://doi.org/10.1021/jp509985u.

65. Bloino J, Biczysko M, Barone V. Anharmonic effects on vibrational spectra intensities: infrared, Raman, vibrational circular dichroism, and Raman optical activity. *J Phys Chem A* 2015, 119:11862–11874. https://doi.org/10.1021/acs.jpca.5b10067.

66. Ramakrishnan R, Rauhut G. Semi-quartic force fields retrieved from multi-mode expansions: accuracy, scaling behavior, and approximations. *J Chem Phys* 2015, 142:154118. https://doi.org/10.1063/1.4918587.

67. Stanton JF, Gauss J, Harding ME, Szalay PG. CFOUR *a quantum chemical program package* with contributions from A. A. Auer, R. J. Bartlett, U. Benedikt, C. Berger, D. E. Bernholdt, Y. J. Bomble, O. Christiansen, M. Heckert, O. Heun, C. Huber, T.-C. Jagau, D. Jonsson, J. Jusélius, K. Klein, W. J. Lauderdale, D. Matthews, T. Metzroth, L. A. Mueck, D. P. O'Neill, D. R. Price, E. Prochnow, C. Puzzarini, K. Ruud, F. Schiffmann, W. Schwalbach, S. Stopkowicz, A. Tajti, J. Vázquez, F. Wang, J. D. Watts and the integral packages Molecule (J. Almloef and P. R. Taylor), PROPS (P. R. Taylor), ABACUS (T. Helgaker, H. J. Aa Jensen, P. Jørgensen, and J. Olsen), and ECP routines by A. V. Mitin and C. van Wüllen, 2011. For the current version, see http://www.cfour.de.

68. DALTON, *a molecular electronic structure program*, Release DALTON2013. 2014. Available at: http://daltonprogram.org.

69. Schmidt MW, Baldridge KK, Boatz JA, Elbert ST, Gordon MS, Jensen JH, Koseki S, Matsunaga N, Nguyen KA, Su S, et al. General atomic and molecular electronic structure system. *J Comput Chem* 1993, 14:1347–1363. https://doi.org/10.1002/jcc.540141112.

70. Gordon MS, Schmidt MW. Advances in electronic structure theory: GAMESS a decade later. In: *Theory and Applications of Computational Chemistry: The First Forty Years*. Elsevier; 2005, 1167–1189.

71. Frisch MJ, Trucks GW, Schlegel HB, Scuseria GE, Robb MA, Cheeseman JR, Scalmani G, Barone V, Petersson GA, Nakatsuji H, et al. *Gaussian 16 Revision A.03*. Wallingford CT: gaussian Inc; 2016.
72. H.-J. Werner, P. J. Knowles, G. Knizia, F. R. Manby, M. Schütz, P. Celani, T. Korona, R. Lindh, A. Mitrushenkov, G. Rauhut, et al., Molpro, version 2012.1, a package of ab initio programs, 2012. Available at: http://www.molpro.net.
73. Valiev M, Bylaska EJ, Govind N, Kowalski K, Straatsma TP, Van Dam HJJ, Wang D, Nieplocha J, Apra E, Windus TL, et al. NWChem: a comprehensive and scalable open-source solution for large scale molecular simulations. *Comput Phys Commun* 2010, 181:1477–1489. https://doi.org/10.1016/j.cpc.2010.04.018.
74. Shao Y, Molnar LF, Jung Y, Kussmann J, Ochsenfeld C, Brown ST, Gilbert AT, Slipchenko LV, Levchenko SV, O'Neill DP, et al. Advances in methods and algorithms in a modern quantum chemistry program package. *Phys Chem Chem Phys* 2006, 8:3172–3191. https://doi.org/10.1039/B517914A.
75. Carbonnière P, Dargelos A, Pouchan C. The VCI-P code: an iterative variation–perturbation scheme for efficient computations of anharmonic vibrational levels and IR intensities of polyatomic molecules. *Theor Chem Accounts* 2010, 125:543–554. https://doi.org/10.1007/s00214-009-0689-7.
76. Watson JK. Simplification of the molecular vibration-rotation hamiltonian. *Mol Phys* 1968, 15:479–490. https://doi.org/10.1080/00268976800101381.
77. Császár AG. Anharmonic molecular force fields. *Wiley Interdiscip Rev Comput Mol Sci* 2011, 2:273–289. https://doi.org/10.1002/wcms.75.
78. Eckart C. Some studies concerning rotating axes and polyatomic molecules. *Phys Rev* 1935, 47:552–558. https://doi.org/10.1103/PhysRev.47.552.
79. Van Vleck JH. One-type doubling and electron spin in the spectra of diatomic molecules. *Phys Rev* 1929, 33:467–506. https://doi.org/10.1103/PhysRev.33.467.
80. Watson JKG. Determination of centrifugal distortion coefficients of asymmetric-top molecules. III. Sextic coefficients. *J Chem Phys* 1968, 48:4517–4524. https://doi.org/10.1063/1.1668020.
81. Watson JKG. In: Durig J, ed. *Vibrational Spectra and Structure*. A Series of Advances, vol. 6. Amsterdam: Elsevier; 1977, 1–89. ISBN: 0-444-41588-2.
82. Vázquez J, Stanton JF. Treatment of Fermi resonance effects on transition moments in vibrational perturbation theory. *Mol Phys* 2007, 105:101–109. https://doi.org/10.1080/00268970601135784.
83. Konen IM, Pollack IB, Li EXJ, Lester MI, Varner ME, Stanton JF. Infrared overtone spectroscopy and unimolecular decay dynamics of peroxynitrous acid. *J Chem Phys* 2005, 122:094320. https://doi.org/10.1063/1.1854094.
84. Bouř P. Anharmonic corrections to vibrational energies of molecules: water and Dideuteriooxirane. *J Phys Chem* 1994, 98:8862–8865. https://doi.org/10.1021/j100087a008.
85. Martin JML, Lee TJ, Taylor PM, François J-P. The anharmonic force field of ethylene, C_2H_4, by means of accurate ab initio calculations. *J Chem Phys* 1995, 103:2589–2602. https://doi.org/10.1063/1.469681.
86. Kuhler KM, Truhlar DG, Isaacson AD. General method for removing resonance singularities in quantum mechanical perturbation theory. *J Chem Phys* 1996, 104:4664–4671. https://doi.org/10.1063/1.471161.
87. Martin JML, Taylor PM. Accurate *ab initio* quartic force field for trans-HNNH and treatment of resonance polyads. *Spectrochim Acta A: Mol Spectrosc* 1997, 53:1039–1050. https://doi.org/10.1016/S1386-1425(96)01869-0.
88. Miani A, Cané E, Palmieri P, Trombetti A, Handy NC. Experimental and theoretical anharmonicity for benzene using density functional theory. *J Chem Phys* 2000, 112:248–259. https://doi.org/10.1063/1.480577.
89. Hänninen V, Halonen L. Calculation of spectroscopic parameters and vibrational overtones of methanol. *Mol Phys* 2003, 101:2907–2916. https://doi.org/10.1080/00268970310001598740.
90. Begue D, Carbonniere P, Pouchan C. Calculations of vibrational energy levels by using a hybrid *ab initio* and DFT quartic force field: application to acetonitrile. *J Phys Chem A* 2005, 109:4611–4616. https://doi.org/10.1021/jp0406114.
91. Cané E, Miani A, Trombetti A. Anharmonic force fields of naphthalene-h_8 and naphthalene-d_8. *J Phys Chem A* 2007, 111:8218–8222. https://doi.org/10.1021/jp071610p.
92. Matthews DA, Stanton JF. Quantitative analysis of Fermi resonances by harmonic derivatives of perturbation theory corrections. *Mol Phys* 2009, 107:213–222. https://doi.org/10.1080/00268970902769463.
93. Hermes MR, Hirata S. Second-order many-body perturbation expansions of vibrational Dyson self-energies. *J Chem Phys* 2013, 139:034111. https://doi.org/10.1063/1.4813123.
94. Krasnoshchekov SV, Isayeva EV, Stepanov NF. Criteria for first- and second-order vibrational resonances and correct evaluation of the Darling-Dennison resonance coefficients using the Canonical Van Vleck perturbation theory. *J Chem Phys* 2014, 141:234114 https://doi.org/10.1063/1.4903927.
95. Darling BT, Dennison DM. The water vapor molecule. *Phys Rev* 1940, 57:128–139. https://doi.org/10.1103/PhysRev.57.128.
96. Lehmann KK. Beyond the x-Krelations. *Mol Phys* 1989, 66:1129–1137. https://doi.org/10.1080/00268978900100751.

97. Matthews DA, Vázquez J, Stanton JF. Calculated stretching overtone levels and Darling–Dennison resonances in water: a triumph of simple theoretical approaches. *Mol Phys* 2007, 105:2659–2666. https://doi.org/10.1080/00268970701618424.

98. Bloino J, Baiardi A, Biczysko M. Aiming at an accurate prediction of vibrational and electronic spectra for medium-to-large molecules: an overview. *Int J Quantum Chem* 2016, 116:1543–1574. https://doi.org/10.1002/qua.25188.

99. Gaw JF, Yamaguchi Y, Schaefer HF, Handy NC. Generalization of analytic energy third derivatives for the RHF closed-shell wave function: Derivative energy and integral formalisms and the prediction of vibration-rotation interaction constants. *J Chem Phys* 1986, 85:5132–5142. https://doi.org/10.1063/1.451707.

100. Colwell SM, Jayatilaka D, Maslen PE, Amos RD, Handy NC. Higher analytic derivatives. I. A new implementation for the third derivative of the SCF energy. *Int J Quantum Chem* 1991, 40:179–199. https://doi.org/10.1002/qua.560400203.

101. P. E. Maslen, D. Jayatilaka, S. M. Colwell, R. D. Amos, and N. C. Handy. Higher analytic derivatives. II. The fourth derivative of self-consistent-field energy. *J Chem Phys* 1991, 95:7409–7417. https://doi.org/10.1063/1.461367.

102. Ringholm M, Jonsson D, Ruud K. A general, recursive, and open-ended response code. *J Comput Chem* 2014, 35:622–633. https://doi.org/10.1002/jcc.23533.

103. Allen WD, Császár AG. On the *ab initio* determination of higher-order force constants at nonstationary reference geometries. *J Chem Phys* 1993, 98:2983–3015. https://doi.org/10.1063/1.464127.

104. Puzzarini C, Biczysko M, Barone V. Accurate harmonic/anharmonic vibrational frequencies for open-shell systems: performances of the B3LYP/N07D model for Semirigid free radicals benchmarked by CCSD(T) computations. *J Chem Theory Comput* 2010, 6:828–838. https://doi.org/10.1021/ct900594h.

105. Császár AG, Allen WD, Schaefer HF III. In pursuit of the *ab initio* limit for conformational energy prototypes. *J Chem Phys* 1998, 108:9751–9764. https://doi.org/10.1063/1.476449.

106. Montgomery JA Jr, Frisch MJ, Ochterski JW, Petersson GA. A complete basis set model chemistry. VI. Use of density functional geometries and frequencies. *J Chem Phys* 1999, 110:2822–2827. https://doi.org/10.1063/1.477924.

107. Tajti A, Szalay PG, Császár AG, Kállay M, Gauss J, Valeev EF, Flowers BA, Vázquez J, Stanton JF. HEAT: high accuracy extrapolated *ab initio* thermochemistry. *J Chem Phys* 2004, 121:11599–11613. https://doi.org/10.1063/1.1811608.

108. Heckert M, Kállay M, Gauss J. Molecular equilibrium geometries based on coupled-cluster calculations including quadruple excitations. *Mol Phys* 2005, 103:2109–2115. https://doi.org/10.1080/00268970500083416.

109. Heckert M, Kállay M, Tew DP, Klopper W, Gauss J. Basis-set extrapolation techniques for the accurate calculation of molecular equilibrium geometries using coupled-cluster theory. *J Chem Phys* 2006, 125:044108. https://doi.org/10.1063/1.2217732.

110. Puzzarini C, Heckert J, Gauss J. The accuracy of rotational constants predicted by high-level quantum-chemical calculations. I. Molecules containing first-row atoms. *J Chem Phys* 2008, 128:194108 https://doi.org/10.1063/1.2912941.

111. Raghavachari K, Trucks GW, Pople JA, Head-Gordon M. A fifth-order perturbation comparison of electron correlation theories. *Chem Phys Lett* 1989, 157:479–483. https://doi.org/10.1016/S0009-2614(89)87395-6.

112. Noga J, Bartlett RJ. The full CCSDT model for molecular electronic structure. *J Chem Phys* 1987, 86:7041–7050. https://doi.org/10.1063/1.452353.

113. Scuseria GE, Schaefer HF III. A new implementation of the full CCSDT model for molecular electronic structure. *Chem Phys Lett* 1988, 152:382–386. https://doi.org/10.1016/0009-2614(88)80110-6.

114. Watts JD, Bartlett RJ. The coupled-cluster single, double, and triple excitation model for open-shell single reference functions. *J Chem Phys* 1990, 93:6104–6105. https://doi.org/10.1063/1.459002.

115. Kállay M, Surján PR. Higher excitations in coupled-cluster theory. *J Chem Phys* 2001, 115:2945–2954. https://doi.org/10.1063/1.1383290.

116. Dunning TH Jr. Gaussian basis sets for use in correlated molecular calculations. I. The atoms boron through neon and hydrogen. *J Chem Phys* 1989, 90:1007–1023. https://doi.org/10.1063/1.456153.

117. Wilson AK, van Mourik T, Dunning TH Jr. Gaussian basis sets for use in correlated molecular calculations. VI. Sextuple zeta correlation consistent basis sets for boron through neon. *J Mol Struct Theochem* 1996, 388:339–349. https://doi.org/10.1016/S0166-1280(96)80048-0.

118. Woon DE, Dunning TH Jr. Gaussian basis sets for use in correlated molecular calculations. V. Core-valence basis sets for boron through neon. *J Chem Phys* 1995, 103:4572–4585. https://doi.org/10.1063/1.470645.

119. Peterson KA, Dunning TH Jr. Accurate correlation consistent basis sets for molecular core–valence correlation effects: the second row atoms Al–Ar, and the first row atoms B–Ne revisited. *J Chem Phys* 2002, 117:10548–10560. https://doi.org/10.1063/1.1520138.

120. Puzzarini C. Rotational spectroscopy meets theory. *Phys Chem Chem Phys* 2013, 15:6595–6607. https://doi.org/10.1039/C3CP44301A.

121. Thorwirth S, Mück LA, Gauss J, Tamassia F, Lattanzi V, McCarthy MC. Silicon Oxysulfide, OSiS: rotational Spectrum, quantum-chemical calculations, and equilibrium structure. *J Phys Chem Lett* 2011, 2:1228–1231. https://doi.org/10.1021/jz200368x.

122. Barone V, Biczysko M, Bloino J, Puzzarini C. Glycine conformers: a never-ending story? *Phys Chem Chem Phys* 2013, 15:1358–1363. https://doi.org/10.1039/C2CP43884D.

123. Puzzarini C, Stanton JF, Gauss J. Quantum-chemical calculation of spectroscopic parameters for rotational spectroscopy. *Int Rev Phys Chem* 2010, 29:273–367. https://doi.org/10.1080/01442351003643401.

124. Martin JM, Taylor PR. The geometry, vibrational frequencies, and total atomization energy of ethylene. A calibration study. *Chem Phys Lett* 1996, 248:336–344. https://doi.org/10.1016/0009-2614(95)01353-9.

125. Demaison J, Margulès L, Boggs JE. The Equilibrium C–Cl, C–Br, and C–I Bond lengths from *ab initio* calculations, microwave and infrared spectroscopies, and empirical correlations. *Struct Chem* 2003, 14:159–174. https://doi.org/10.1023/A:1022138431967.

126. Puzzarini C. Extrapolation to the complete basis set limit of structural parameters: comparison of different approaches. *J Phys Chem A* 2009, 113:14530–14535. https://doi.org/10.1021/jp9040327.

127. Puzzarini C, Barone V. Extending the molecular size in accurate quantum-chemical calculations: the equilibrium structure and spectroscopic properties of uracil. *Phys Chem Chem Phys* 2011, 13:7189–7197. https://doi.org/10.1039/C0CP02636K.

128. Møller C, Plesset MS. Note on an approximation treatment for many-electron systems. *Phys Rev* 1934, 46:618–622. https://doi.org/10.1103/PhysRev.46.618.

129. Puzzarini C, Biczysko M, Barone V, Pena I, Cabezas C, Alonso JL. Accurate molecular structure and spectroscopic properties of nucleobases: a combined computational–microwave investigation of 2-thiouracil as a case study. *Phys Chem Chem Phys* 2013, 15:16965–16975. https://doi.org/10.1039/C3CP52347K.

130. Helgaker T, Klopper W, Koch H, Noga J. Basis-set convergence of correlated calculations on water. *J Chem Phys* 1997, 106:9639–9646. https://doi.org/10.1063/1.473863.

131. Pietropolli Charmet A, Stoppa P, Giorgianni S, Bloino J, Tasinato N, Carnimeo I, Biczysko M, Puzzarini C. Accurate vibrational–rotational parameters and infrared intensities of 1-Bromo-1-fluoroethene: a joint experimental analysis and ab initio study. *J Phys Chem A* 2017, 121:3305–3317. https://doi.org/10.1021/acs.jpca.7b02060.

132. Puzzarini C, Cazzoli G, Gauss J. The rotational spectra of $HD^{17}O$ and $D_2{}^{17}O$: experiment and quantum-chemical calculations. *J Chem Phys* 2012, 137:154311 https://doi.org/10.1063/1.4758316.

133. Puzzarini C, Biczysko M, Barone V. Accurate Anharmonic vibrational frequencies for uracil: the performance of composite schemes and hybrid CC/DFT model. *J Chem Theory Comput* 2011, 7:3702–3710. https://doi.org/10.1021/ct200552m.

134. Puzzarini C, Penocchio E, Biczysko M, Barone V. Molecular structure and spectroscopic signatures of acrolein: theory meets experiment. *J Phys Chem A* 2014, 118:6648–6656. https://doi.org/10.1021/jp503672g.

135. Burke K. Perspective on density functional theory. *J Chem Phys* 2012, 136:150901 https://doi.org/10.1063/1.4704546.

136. Becke AD. Density-functional thermochemistry. III. The role of exact exchange. *J Chem Phys* 1993, 98:5648–5652. https://doi.org/10.1063/1.464913.

137. Grimme S. Semiempirical hybrid density functional with perturbative second-order correlation. *J Chem Phys* 2006, 124:034108. https://doi.org/10.1063/1.2148954.

138. Pulay P, Meyer W, Boggs JE. Cubic force constants and equilibrium geometry of methane from Hartree--Fock and correlated wavefunctions. *J Chem Phys* 1978, 68:5077–5085. https://doi.org/10.1063/1.435626.

139. Pawlowski F, Jørgensen P, Olsen J, Hegelund F, Helgaker T, Gauss J, Bak KL, Stanton JF. Molecular equilibrium structures from experimental rotational constants and calculated vibration–rotation interaction constants. *J Chem Phys* 2002, 116:6482–6496. https://doi.org/10.1063/1.1459782.

140. Demaison J, Boggs JE, Császár AG. *Equilibrium Molecular Structures: From Spectroscopy to Quantum Chemistry*. Boca Raton, FL: CRC Press; 2010. ISBN: 9781439811351 Available at: https://books.google.it/books?id=7DZB0ITw0BsC.

141. Piccardo M, Penocchio E, Puzzarini C, Biczysko M, Barone V. Semi-experimental equilibrium structure determinations by employing B3LYP/SNSD Anharmonic force fields: validation and application to Semi-rigid organic molecules. *J Phys Chem A* 2015, 119:2058–2082. https://doi.org/10.1021/jp511432m.

142. Biczysko M, Bloino J, Brancato G, Cacelli I, Cappelli C, Ferretti A, Lami A, Monti S, Pedone A, Prampolini G, et al. Integrated computational approaches for spectroscopic studies of molecular systems in the gas phase and in solution: pyrimidine as a test case. *Theor Chem Accounts* 2012, 131:1–19. https://doi.org/10.1007/s00214-012-1201-3.

143. Barone V, Biczysko M, Bloino J, Puzzarini C. Characterization of the elusive conformers of glycine from state-of-the-art structural, thermodynamic, and

spectroscopic computations: theory complements experiment. *J Chem Theory Comput* 2013, 9:1533–1547. https://doi.org/10.1021/ct3010672.

144. Fornaro T, Biczysko M, Monti S, Barone V. Dispersion corrected DFT approaches for anharmonic vibrational frequency calculations: nucleobases and their dimers. *Phys Chem Chem Phys* 2014, 16:10112–10128. https://doi.org/10.1021/jp510101y.
145. Penocchio E, Piccardo M, Barone V. Semiexperimental equilibrium structures for building blocks of organic and biological molecules: the B2PLYP route. *J Chem Theory Comput* 2015, 11:4689–4707. https://doi.org/10.1021/acs.jctc.5b00622.
146. Biczysko M, Panek P, Scalmani G, Bloino J, Barone V. Harmonic and anharmonic vibrational frequency calculations with the double-hybrid B2PLYP method: analytic second derivatives and benchmark studies. *J Chem Theory Comput* 2010, 6:2115–2125. https://doi.org/10.1021/ct100212p.
147. Carnimeo I, Puzzarini C, Tasinato N, Stoppa P, Pietropolli Charmet A, Biczysko M, Cappelli C, Barone V. Anharmonic theoretical simulations of infrared spectra of halogenated organic compounds. *J Chem Phys* 2013, 139:074310. https://doi.org/10.1063/1.4817401.
148. Bernard J-M, Coll P, Coustenis A, Raulin F. Experimental simulation of Titan's atmosphere: detection of ammonia and ethylene oxide. *Planet Space Sci* 2003, 51:1003–1011. https://doi.org/10.1016/j.pss.2003.05.009.
149. Coll P, Bernard J-M, Navarro-Gonzalez R, Raulin F. Oxirane: an exotic oxygenated organic compound on Titan? *Astrophys J* 2003, 598:700–703. https://doi.org/10.1086/378792.
150. Bennet CJ, Osamura Y, Lebar MD, Kaiser RI. Laboratory studies on the formation of three C_2H_4O isomers—acetaldehyde (CH_3CHO), ethylene oxide (c-C_2H_4O), and vinyl alcohol (CH_2CHOH)—in interstellar and cometary ices. *Astrophys J* 2005, 634:698–711. https://doi.org/10.1086/452618.
151. Bernstein LS, Lynch DK. Small carbonaceous molecules, ethylene oxide (c-C_2H_4O) and cyclopropenylidene (c-C_3H_2): sources of the unidentified infrared bands? *Astrophys J* 2009, 704:226–239. https://doi.org/10.1088/0004-637X/704/1/226.
152. Puzzarini C, Ali A, Biczysko M, Barone V. Accurate spectroscopic characterization of protonated Oxirane: a potential prebiotic species in Titan's atmosphere. *Astrophys J* 2014, 792:118 https://doi.org/10.1088/0004-637X/792/2/118.
153. Mesko A, Zou L, Carroll PB, Weaver SLW. Millimeter and submillimeter spectrum of propylene oxide. *J Mol Spectrosc* 2017, 335:49–53. https://doi.org/10.1016/j.jms.2017.02.003.
154. Medcraft C, Thompson CD, Robertson EG, Appadoo DRT, McNaughton D. The far-infrared rotational spectrum of ethylene oxide. *Astrophys J* 2012, 753:18 https://doi.org/10.1088/0004-637X/753/1/18.
155. Lafferty WJ, Flaud JM, Kwabia Tchana F, Fernandez JM. Raman and infrared spectra of the ν_1 band of oxirane. *Mol Phys* 2013, 111:1983–1986. https://doi.org/10.1080/00268976.2013.775516.
156. Tchana FK, Ngom M, Perrin A, Flaud J-M, Lafferty W, Ndiaye S, Ngom E. Absolute line intensities for oxirane from 1420 to 1560 cm^{-1}. *J Mol Spectrosc* 2013, 292:1–4. https://doi.org/10.1016/j.jms.2013.07.006.
157. Flaud J-M, Lafferty W, Tchana FK, Perrin A, Landsheere X. First high-resolution analysis of the ν_{15}, ν_{12}, ν_5, ν_{10} and ν_2 bands of oxirane. *J Mol Spectrosc* 2012, 271:38–43. https://doi.org/10.1016/j.jms.2011.11.005.
158. Nakanaga T. Infrared band intensities of ethylene oxide. *J Chem Phys* 1981, 74:5384–5392. https://doi.org/10.1063/1.440967.
159. Russell DK, Wesendrup R. Tunable diode laser study of the ν_3 band of oxirane. *J Mol Spectrosc* 2003, 217:59–71. https://doi.org/10.1016/S0022-2852(02)00010-3.
160. Tchana FK, Flaud J-M, Lafferty W, Ngom M. Absolute line intensities for oxirane in the 11.4 μm spectral region. *Mol Phys* 2014, 112:1633–1638. https://doi.org/10.1080/00268976.2013.851811.
161. Sloan GC, Kraemer KE, Price SD, Shipman RF. A uniform database of 2.4–45.4 micron spectra from the infrared space observatoryshort wavelength spectrometer. *Astrophys J Suppl Ser* 2003, 147:379–401. https://doi.org/10.1086/375443.
162. Bernard Salas J, Pottasch SR, Beintema DA, Wesselius PR. The ISO-SWS spectrum of planetary nebula NGC 7027. *Astron Astrophys* 2001, 367:949–958. https://doi.org/10.1051/0004-6361:20000435.
163. Kwok S, Zhang Y. Mixed aromatic–aliphatic organic nanoparticles as carriers of unidentified infrared emission features. *Nature* 2011, 479:80–83. https://doi.org/10.1038/nature10542.
164. Tercero B, Kleiner I, Cernicharo J, Nguyen HVL, López A, Muñoz Caro GM. Discovery of methyl acetate and Gauche ethyl formate in Orion. *Astrophys J Lett* 2013, 770:L13. https://doi.org/10.1088/2041-8205/770/1/L13.
165. Bellili A, Linguerri R, Hochlaf M, Puzzarini C. Accurate structural and spectroscopic characterization of prebiotic molecules: the neutral and cationic acetyl cyanide and their related species. *J Chem Phys* 2015, 143:184314 https://doi.org/10.1063/1.4935493.
166. Kraśnicki A, Pszczółkowski L, Kisiel Z. Analysis of the rotational spectrum of pyruvonitrile up to 324 GHz. *J Mol Spectrosc* 2010, 260:57–65. https://doi.org/10.1016/j.jms.2009.12.005.

167. Mitrushchenkov AO. A new general Renner-teller (including $\gtrsim 1$) spectroscopic formalism for triatomic molecules. *J Chem Phys* 2012, 136:024108. https://doi.org/10.1063/1.3672162.

168. Panek PT, Jacob CR. On the benefits of localized modes in anharmonic vibrational calculations for small molecules. *J Chem Phys* 2016, 144:164111 https://doi.org/10.1063/1.4947213.

169. König C, Hansen MB, Godtliebsen IH, Christiansen O. FALCON: a method for flexible adaptation of local coordinates of nuclei. *J Chem Phys* 2016, 144:074108. https://doi.org/10.1063/1.4941846.

170. Cheng X, Talbot JJ, Steele RP. Tuning vibrational mode localization with frequency windowing. *J Chem Phys* 2016, 145:124112 https://doi.org/10.1063/1.4963109.

171. Pulay P, Fogarasi G, Pang F, Boggs JE. Systematic ab initio gradient calculation of molecular geometries, force constants, and dipole moment derivatives. *J Am Chem Soc* 1979, 101:2550–2560. https://doi.org/10.1021/ja00504a009.

172. Baiardi A, Bloino J, Barone V. Simulation of Vibronic spectra of flexible systems: hybrid DVR-harmonic approaches. *J Chem Theory Comput* 2017, 13:2804–2822. https://doi.org/10.1021/acs.jctc.7b00236.

173. Miller WH, Handy NC, Adams JE. Reaction path Hamiltonian for polyatomic molecules. *J Chem Phys* 1980, 72:99–112. https://doi.org/10.1063/1.438959.

174. Carrington T, Miller WH. Reaction surface Hamiltonian for the dynamics of reactions in polyatomic systems. *J Chem Phys* 1984, 81:3942–3950. https://doi.org/10.1063/1.448187.

175. Barone V, Minichino C. From concepts to algorithms for the treatment of large amplitude internal motions and unimolecular reactions. *J Mol Struct Theochem* 1995, 330:365–376. https://doi.org/10.1016/0166-1280(94)03862-F.

176. Tew DP, Handy NC, Carter S. A reaction surface Hamiltonian study of malonaldehyde. *J Chem Phys* 2006, 125:084313. https://doi.org/10.1063/1.2338891.

177. Tew DP, Handy NC, Carter S. Glyoxal studied with 'multimode', explicit large amplitude motion and anharmonicity. *Phys Chem Chem Phys* 2001, 3:1958–1964. https://doi.org/10.1039/B101631H.

178. Senent ML, Puzzarini C, Dominguez-Gomez R, Carvajal M, Hochlaf M. Theoretical spectroscopic characterization at low temperatures of detectable sulfur-organic compounds: ethyl mercaptan and dimethyl sulfide. *J Chem Phys* 2014, 140:124302 https://doi.org/10.1063/1.4868640.

179. Cologne Database for Molecular Spectroscopy: glycine, aminoacetic acid, conformer II. Available at: https://www.astro.uni-koeln.de/cgi-bin/cdmsinfo?file=e075512.cat. (Accessed May 5, 2017).

180. Jimenez-Serra I, Testi L, Caselli P, Viti S. Detectability of glycine in solar-type system precursors. *Astrophys J Lett* 2014, 787:L33 https://doi.org/10.1088/2041-8205/787/2/L33.

181. Garrod RT. A three-phase chemical model of hot cores: the formation of glycine. *Astrophys J* 2013, 765:60. https://doi.org/10.1088/0004-637X/765/1/60.

182. Császár AG. Conformers of gaseous glycine. *J Am Chem Soc* 1992, 114:9568–9575. https://doi.org/10.1021/ja00050a041.

183. Bazso G, Magyarfalvi G, Tarczay G. Near-infrared laser induced conformational change and UV laser photolysis of glycine in low-temperature matrices: observation of a short-lived conformer. *J Mol Struct* 2012, 1025:33–42. https://doi.org/10.1016/j.molstruc.2012.04.066.

184. Bazso G, Magyarfalvi G, Tarczay G. Tunneling lifetime of thettc/VIp conformer of glycine in low-temperature matrices. *J Phys Chem A* 2012, 116:10539–10547. https://doi.org/10.1021/jp3076436.

185. Ayala PY, Schlegel HB. Identification and treatment of internal rotation in normal mode vibrational analysis. *J Chem Phys* 1998, 108:2314–2325. https://doi.org/10.1063/1.475616.

186. Zheng J, Yu T, Papajak E, Alecu IM, Mielke SL, Truhlar DG. Practical methods for including torsional anharmonicity in thermochemical calculations on complex molecules: the internal-coordinate multi-structural approximation. *Phys Chem Chem Phys* 2011, 13:10885–10907. https://doi.org/10.1039/C0CP02644A.

187. Zheng J, Truhlar DG. Including torsional anharmonicity in canonical and microcanonical reaction path calculations. *J Chem Theory Comput* 2013, 9:2875–2881. https://doi.org/10.1021/ct400231q.

188. Skouteris D, Calderini D, Barone V. Methods for calculating partition functions of molecules involving large amplitude and/or anharmonic motions. *J Chem Theory Comput* 2016, 12:1011–1018. https://doi.org/10.1021/acs.jctc.5b01094.

189. Truhlar DG, Isaacson AD. Simple perturbation theory estimates of equilibrium constants from force fields. *J Chem Phys* 1991, 94:357–359. https://doi.org/10.1063/1.460350.

190. Stepanian SG, Reva ID, Radchenko ED, Rosado MTS, Duarte MLTS, Fausto R, Adamowicz L. Matrix-isolation infrared and theoretical studies of the glycine conformers. *J Phys Chem A* 1998, 102:1041–1054. https://doi.org/10.1021/jp973397a.

191. Chyba C, Sagan C. Endogenous production, exogenous delivery and impact-shock synthesis of organic molecules: an inventory for the origins of life. *Nature* 1992, 355:125–132. https://doi.org/10.1038/355125a0.

192. Miller SL. A production of amino acids under possible primitive earth conditions. *Science* 1953, 117:528–529. https://doi.org/10.1126/science.117.3046.528.

193. Miller SL, Urey HC. Organic compound synthes on the primitive Eart: several questions about the origin of life have been answered, but much remains to be studied. *Science* 1959, 130:245–251. https://doi.org/10.1126/science.130.3370.245.

194. Raulin F, McKay C, Lunine J, Owen T. *Titan's Astrobiology*. Dordrecht: Springer; 2010, 215–233. ISBN: 978-1-4020-9215-2.

195. Barone V, Latouche C, Skouteris D, Vazart F, Balucani N, Ceccarelli C, Lefloch B. Gas-phase formation of the prebiotic molecule formamide: insights from new quantum computations. *Mon Not R Astron Soc Lett* 2015, 453:L31–L35. https://doi.org/10.1093/mnrasl/slv094.

196. Skouteris D, Vazart F, Ceccarelli C, Balucani N, Puzzarini C, Barone V. New quantum chemical computations of formamide deuteration support gas-phase formation of this prebiotic molecule. *Mon Not R Astron Soc Lett* 2017, 468:L1. https://doi.org/10.1093/mnrasl/slx012.

197. Klippenstein SJ, Pande VS, Truhlar DG. Chemical kinetics and mechanisms of complex systems: a perspective on recent theoretical advances. *J Am Chem Soc* 2014, 136:528–546. https://doi.org/10.1021/ja408723a.

198. Truhlar DG, Garrett BC, Klippenstein SJ. Current status of transition-state theory. *J Phys Chem* 1996, 100:12771–12800. https://doi.org/10.1021/jp953748q.

199. Nguyen TL, Stanton JF, Barker JR. Ab initio reaction rate constants computed using semiclassical transition-state theory: HO + H_2 → H_2O + H and Isotopologues. *J Phys Chem A* 2011, 115:5118–5126. https://doi.org/10.1021/jp2022743.

200. Peters B, Bell AT, Chakraborty A. Rate constants from the reaction path Hamiltonian. II. Nonseparable semiclassical transition state theory. *J Chem Phys* 2004, 121:4461–4466. https://doi.org/10.1063/1.1778162.

201. Bacmann A, Taquet V, Faure A, Kahane C, Ceccarelli C. Detection of complex organic molecules in a prestellar core: a new challenge for astrochemical models. *Astron Astrophys* 2012, 541:L12 https://doi.org/10.1051/0004-6361/201219207.

202. Saladino R, Botta G, Pino S, Costanzo G, Di Mauro E. Genetics first or metabolism first? The formamide clue. *Chem Soc Rev* 2012, 41:5526–5565. https://doi.org/10.1039/C2CS35066A.

203. Grimme S, Antony J, Ehrlich S, Krieg H. A consistent and accurate *ab initio* parametrization of Density Functional Dispersion Correction (DFT-D) for the 94 elements H-Pu. *J Chem Phys* 2010, 132:154104 https://doi.org/10.1063/1.3382344.

204. Ali A, Sittler E Jr, Chornay D, Rowe B, Puzzarini C. Organic chemistry in Titan's upper atmosphere and its astrobiological consequences: I. Views towards Cassini plasma spectrometer (CAPS) and ion neutral mass spectrometer (INMS) experiments in space. *Planet Space Sci* 2015, 109–110:46–63. https://doi.org/10.1016/j.pss.2015.01.015.

205. Ten GN, Nechaev VV, Krasnoshchekov SV. Interpretation of vibrational IR spectrum of uracil using anharmonic calculation of frequencies and intensities in second-order perturbation theory. *Opt Spectrosc* 2010, 108:37–44. https://doi.org/10.1134/S0030400X10010078.